Copyright Warning & Restrictions

The copyright law of the United States (Title 17, United States Code) governs the making of photocopies or other reproductions of copyrighted material.

Under certain conditions specified in the law, libraries and archives are authorized to furnish a photocopy or other reproduction. One of these specified conditions is that the photocopy or reproduction is not to be "used for any purpose other than private study, scholarship, or research." If a, user makes a request for, or later uses, a photocopy or reproduction for purposes in excess of "fair use" that user may be liable for copyright infringement,

This institution reserves the right to refuse to accept a copying order if, in its judgment, fulfillment of the order would involve violation of copyright law.

Please Note: The author retains the copyright while the New Jersey Institute of Technology reserves the right to distribute this thesis or dissertation

Printing note: If you do not wish to print this page, then select "Pages from: first page # to: last page #" on the print dialog screen

ABSTRACT

CONTROL OF SMART STRUCTURE USING ADAPTIVE DITHER

by
Tian Hong

In this thesis, a mathematical model of a piezoelectric stack actuator is presented to describe its voltage versus displacement hysteresis characteristices. This model can accommodate a wide range of piezoelectric materials, including the PZT (lead zirconate—lead titanate) type which is most popular in industrial applications.

Besides describing the conventional "single-loop" hysteresis, this model also accounts for the off-axis minor loops by augmenting the algorithm with loop indexing.

It is shown that the PZT hysteresis possesses certain "weak scalability" that enables the use of spectral analysis to measure the level of nonlinearity.

After a suitable mathematical model has been obtained, a dither is injected into the model to weaken the nonlinearity of hysteresis loop. An integral controller and a harmonic ratio comparator are used in an adaptive system to determine suitable dither amplitude to meet the requirement of the reference distortion lever. The dither effectively "linearizes" the hysteresis nonlinearity, thus rendering it more suitable for application to precision control.

Extensive numerical simulations are carried out and simulation results are presented.

CONTROL OF SMART STRUCTURE USING ADAPTIVE DITHER

by
Tian Hong

A Thesis
Submitted to the Faculty of
New Jersey Institute of Technology
in Partial Fulfillment of the Requirements for the Degree of
Master of Science in Electrical and Computer Engineering

Department of Electrical and Computer Engineering

October 1994

APPROVAL PAGE

CONTROL OF SMART STRUCTURE USING ADAPTIVE DITHER

Tian Hong

Dr. Timothy Chang, Thesis Advisor Assitant Professor of Electrical and Computer Engineering, NJIT	Date
Dr. Andrew Meyer, Committee Member Professor of Electrical and Computer Engineering, NJIT	Date
Dr. Edwin Hou, Committee Member Assistant Professor of Electrical and Computer Engineering, NJIT	Date

BIOGRAPHICAL SKETCH

Author: Tian Hong

Degree: Master of Science in Electrical and Computer Engineering

Date: October 1994

Undergraduate and Graduate Education:

- Master of Science in Electrical Engineering,
  New Jersey Institute of Technology, Newark, NJ, 1994
- Bachelor of Science in Electrical Engineering,
  Shanghai University of Techology, Shanghai, P. R. China, 1989

Major: Electrical and Computer Engineering

This thesis is dedicated to
my family

ACKNOWLEDGMENT

I wish to express my sincere thanks to Dr. Timothy N. Chang, my advisor for his guidance and care throughout my master's program and finacial support during my study and research.

Many thanks also to Dr. Andrew Meyer and Dr. Edwin Hou for serving as members of the committee.

Finally I would like to thank my parents for their great encourgement and finacial support and all my friends for their assistance in whatever they could during the entire work of my thesis.

TABLE OF CONTENTS

LIST OF TABLES

Table Page

LIST OF FIGURES

Figure Page

CHAPTER 1

INTRODUCTION

Piezoelectricity means "pressure electricity". It was discovered by Pierre and Jacques Curies in the 1880's. Piezoelectricity is a property of certain crystals such as quartz, Rochelle salt, tourmaline, barium titanate and many others, those crystals when compressed in certain directions show positive and negative charges on certain portion of their surfaces. The charges are proportional to the pressure and disappear when the pressure is withdrawn. Conversely, when an electric field is applied to one of those materials, there will be dimensional changes in those crystals. Because of this unique electromechanical property, these materials are also called "smart materials". Recently, piezoelectric crystals are being used or are being considered for use as actuators in micro-positioning application, notably in electron-optical system and precision control system. For example, H. S. Tzou in 1987 used it as a sensor and actuator in active vibration control of flexible structure[6], E. F. Grawley in 1987 used piezoelectric actuators as elements of intelligent structures[3] , S. Halevi in 1983 used this smart structure in bimorph piezoelectric flexible mirror in graphical solution and compensation[4] etc.

While the application of smart materials are receiving more and more attention, some problems also appear. A major drawback of usage of these smart materials has been the inability to accurately predict the actuator output position for an arbitrary input voltage. Such shortcoming is due to the lack of a good mathematical model that describes the hysteretic behavior of the crystals as they are actuated, especially when off axis hysteresis minor loops are involved.

The organization of this thesis is as follows:

In Chapter 2, a suitable mathematical model for hysteresis loop is presented, it is based on Philip R. Dahl's solid fraction model (SFM) [2] and augmented by the Prandtl Laws to account for the minor hysteresis loops. Analytic and simulation results are presented. All simulations are carried out on SIMULINK for Windows version 1.2 and Matlab 3.5 of MathWorks Inc. The simulation results confirmed the validity of the model.

In Chapter 3, after obtaining a suitable mathematical model to describe the hysteretic behavior of PZT materials, an adaptive dither signal is injected into the system to smooth out the nonlinearity so as to improve control accuracy and transient dynamics. A controller together with dither signal are applied to regulate the characteristics of the system. This proposed system is shown in Figure 1.1 where the hysteresis model block represents the hysteresis model and A is the amplitude of dither($A \sin \omega_2 t$, where $\omega_2 \geq 10\omega_1$, ω_1 is the input signal frequency). A is varied until a prespecified level of harmonic distortion ratio is satisfied. From an input-output point of view, the dithered system inside the dash block can be considered as a black box so that Figure 1.1 can be redrawn as Figure 1.2. In Chapter 3, it will be shown that the output Y of black box is "linear" to the input U.

In Chapter 4, shape control of PZT materials is presented. Errors due to step response of square wave are compared by simulation results with/without dither. Off-axis minor loops by the neutralization of the adaptive dither will also be demonstrated.

Finally, in Chapter 5, a conclusion of this work is provided together with directions for future research.

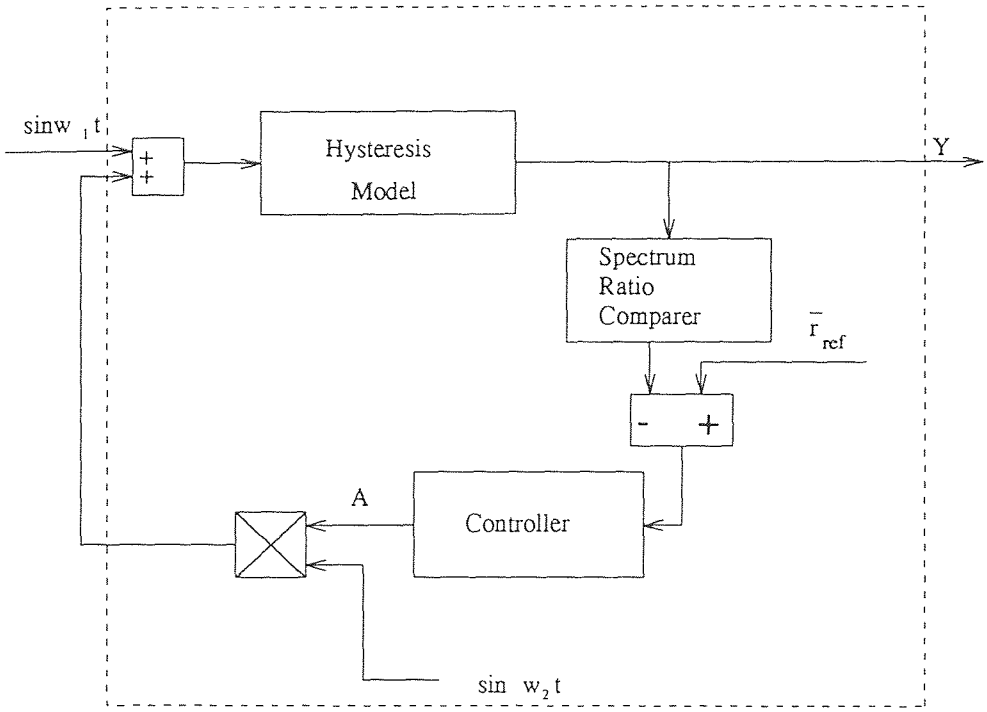

Figure 1.1 System controlled by variable dither

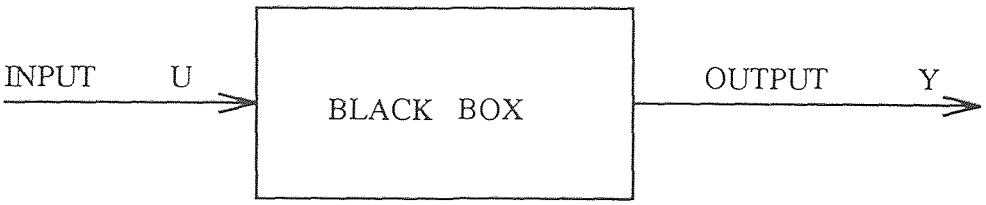

Figure 1.2 Simplified system

CHAPTER 2

MODELING OF PZT HYSTERESIS

In this chapter a hysteresis algorithm is presented which is based on Philip R. Dahl's solid friction model (SFM) [1][2]. In this approach single hysteresis loop formed between applied voltage and mechanical displacement is first considered. This is followed by adding loop index into the algorithm to deal with the off-axis minor loops.

2.1 Single Hysteresis Loop

It is well known that the displacement—voltage relation of PZT materials is nonlinear with various degrees of hysteresis. The solid friction model, pioneered by Philip R. Dahl [1][2], has been considered as a successful model in describing the hysteresis characteristics. The model is given by the following nonlinear differential equation:

$$\frac{dF}{dt} = \frac{dF}{dx}\frac{dx}{dt} \tag{2.1}$$

$$\frac{dF}{dx} = \sigma|1 - \frac{F}{F_c}SGN(\dot{x})|^i SGN(1 - \frac{F}{F_c}SGN(\dot{x})) \tag{2.2}$$

where SGN is sign function:

$$SGN(X) = \begin{cases} 1 & for \quad X \geq 0; \\ -1 & for \quad X < 0; \end{cases}$$

where F is a solid friction force which is a function of displacement x and velocity $\dot{x}$. F has the characteristic as shown in Figure 2.1. The friction force F monotonically approaches $+F_c$ as long as $\dot{x}$ is positive. While $\dot{x} < 0$, F follows the negative of it's original shape and approaches $-F_c$. The friction function slope dF/dx, however, always remains positive even though $\dot{x}$ changes sign. F_c is the Coulomb friction

force which can also be though of as a "yield force" or as "running friction force"(for example, as found in bearing friction).

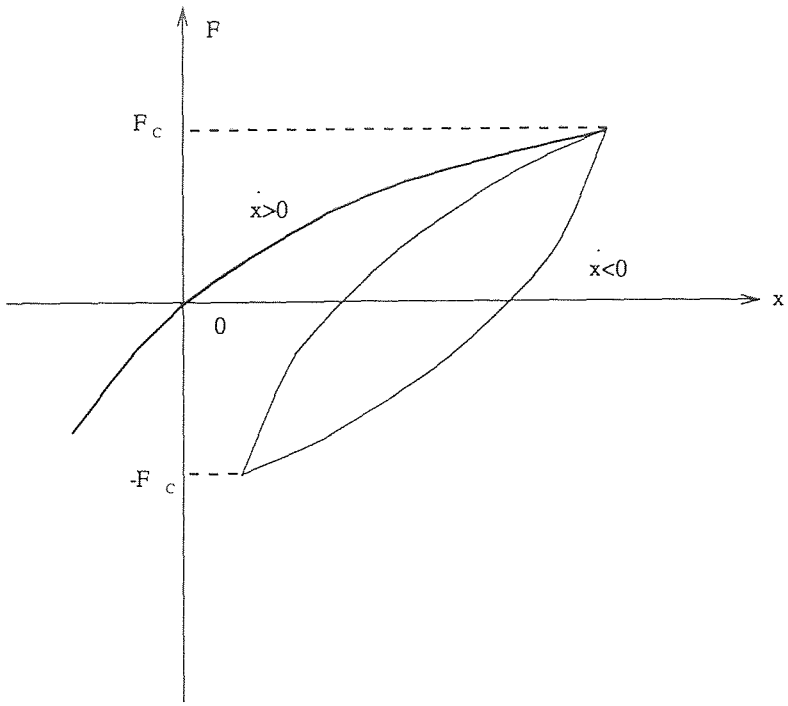

Figure 2.1 Typical solid friction force function

σ is the rest stiffness or slope of the force deflection curve at $F = 0$. The effect of varying σ is shown in Figure 2.2. It is noted as σ increases, the slope of the hysteresis loop increases proportionally and shape of hysteresis loop slightly rotates counterclockwise. In Figure 2.2 the solid line hysteresis loop is for $\sigma = 1$, pointed line(••••) is for $\sigma = 2$, dashed line is for $\sigma = 5$ and dotted line(····) is for $\sigma = 10$. The variable i is a parameter of the type of different crystals, for ductile type $i = 1, 2$, for brittle type $i = 0$, 1/4,1/2. When i is decreased, the hysteresis loop becomes "slim" and slightly rotates counterclockwise as shown in Figure 2.3. The solid line hysteresis loop is for $i = 2$, pointed line is for $i = 1$, dashed line is for $i = 0.5$ and dotted line is for $\sigma = 0.25$. For most PZT materials $\sigma = 1$, $i = 1$, and (2.2) can be simplified to:

$$\frac{dF}{dx} = 1 - \frac{F}{F_c} SGN(\dot{x}) \tag{2.3}$$

The system to be modeled is a PZT stack consisting of 55 PZT discs, each disc is 1.17 cm diameter, 0.18 cm thick and wired in parallel, the model to be simulated is shown in Figure 2.4.

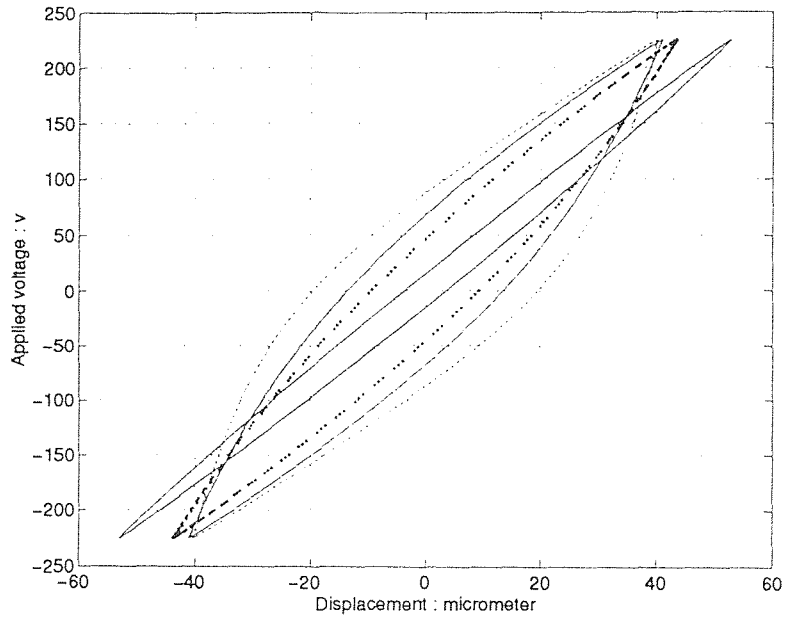

Figure 2.2 Hysteresis loop when $\sigma = 1, 2, 5, 10$

The acceleration of the load mass M is:

$$\ddot{x} = F_A/M \tag{2.4}$$

$$F_A = \frac{NA(1+b)d_{33}}{HS_{33}} V - \gamma\dot{x} - \frac{A}{HS_{33}} x - F \tag{2.5}$$

where:

V: voltage applied to all crystals

x: actuator end displacement

b: fraction of stack height in cement($b \approx 0$)

N: number of discs in PZT stack ($N = 55$)

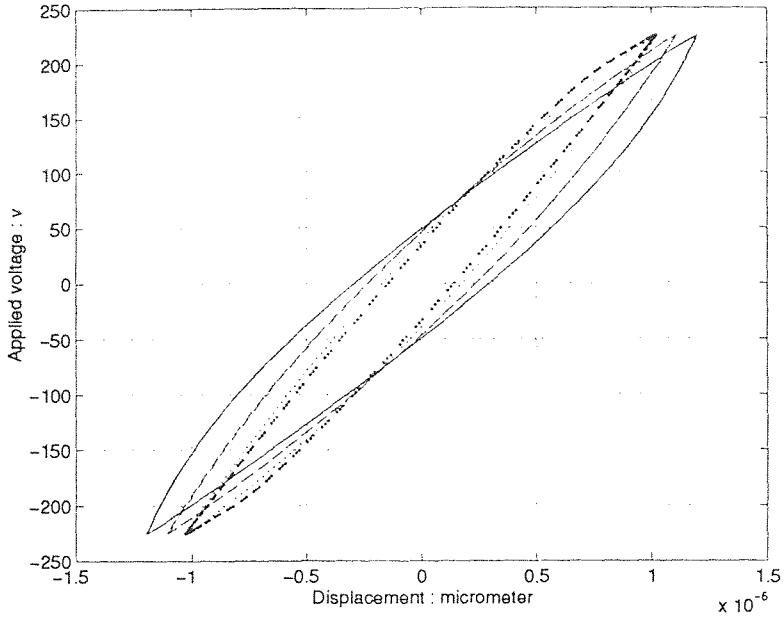

Figure 2.3 Hysteresis loop when $i = 0.25, 0.5, 1, 2$

A: area of disc of PZT stack ($A \approx 4.30 \times 10^{-4}\ m^2$)

d_{33}: crystal strain per electric field coefficient ($d_{33} \approx 500 \times 10^{-12}\ m/v$)

S_{33}: crystal strain per stress coefficient ($S_{33} \approx 20.8 \times 10^{-12}\ m^2/N$)

H: stack height ($H \approx 10\ cm$)

F_A: accelerating force on the load mass

γ: damping coefficient

The diagram of piezo-electric stack actuator model is shown in Figure 2.5. Clearly from the block diagram, the system consists of two parts:

(A) Linear part:

$$F_A = \frac{NA(1+b)d_{33}}{HS_{33}}V - \gamma\dot{x} - \frac{A}{HS_{33}}x \tag{2.6}$$

(B)Nonlinear part:

$$\frac{dF}{dx} = 1 - \frac{F}{F_c}SGN(\dot{x}) \tag{2.7}$$

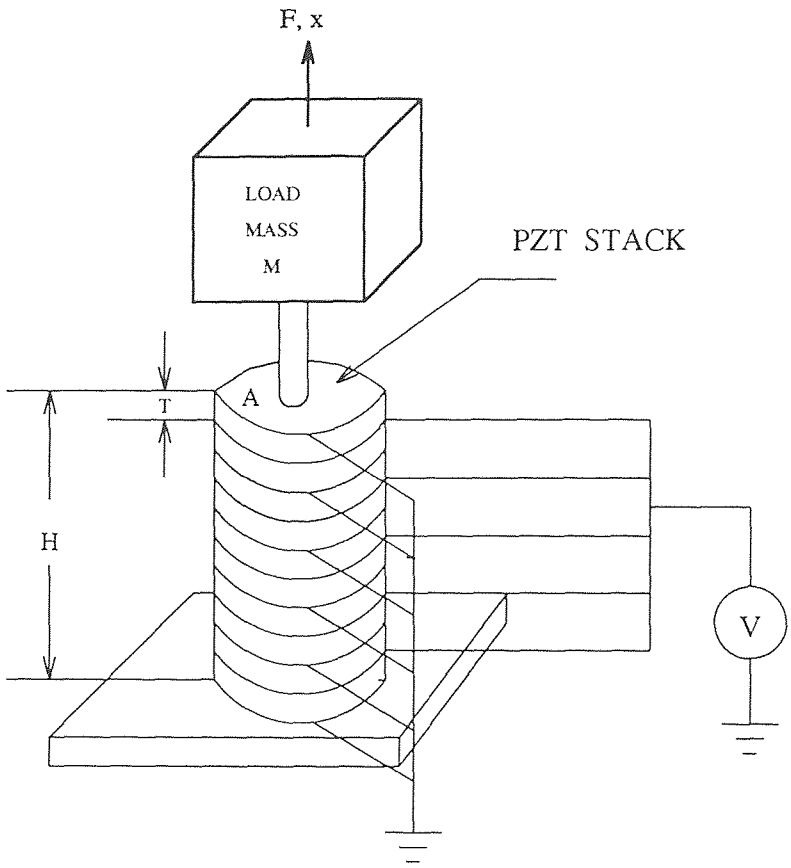

Figure 2.4 PZT pieozo-electric stack actuator

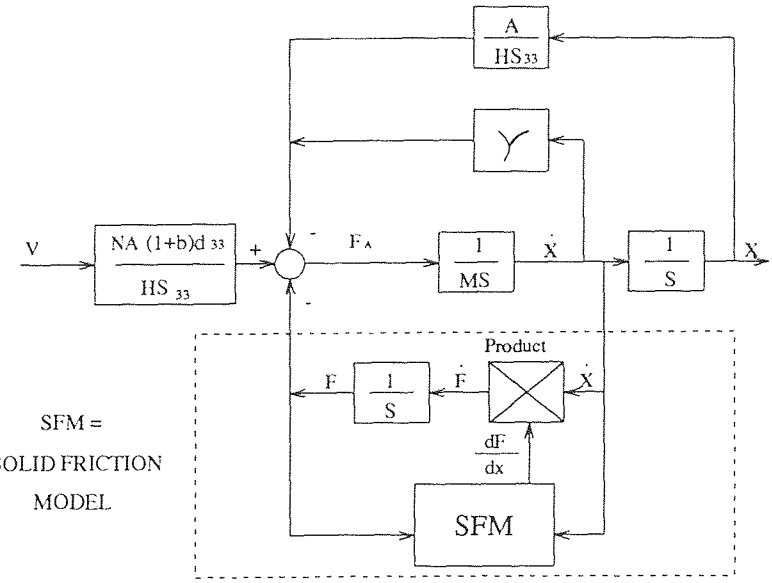

Figure 2.5 Block diagram of piezo-electric stack actuator model

It is obvious that the whole system is a second order linear system affected by a nonlinear force F. The corresponding simulation diagram is shown in Figure 2.6. The model now becomes

$$F_A = K_V V - \gamma \dot{x} - K_N x - K_1 F \tag{2.8}$$

Where

$$K_V = \frac{NA(1+b)d_{33}}{HS_{33}}, \qquad K_N = \frac{A}{HS_{33}} \tag{2.9}$$

K_V and K_N are, respectively, the voltage-force scale factor and the equivalent spring rate. They are determined by the type and shape of the smart materials. For the particular PZT system,

$$K_V = \frac{NA(1+b)d_{33}}{HS_{33}} \approx 5.8300 \quad N/V \tag{2.10}$$

$$K_N = \frac{A}{HS_{33}} \approx 2.01944 \times 10^8 \quad N/m \tag{2.11}$$

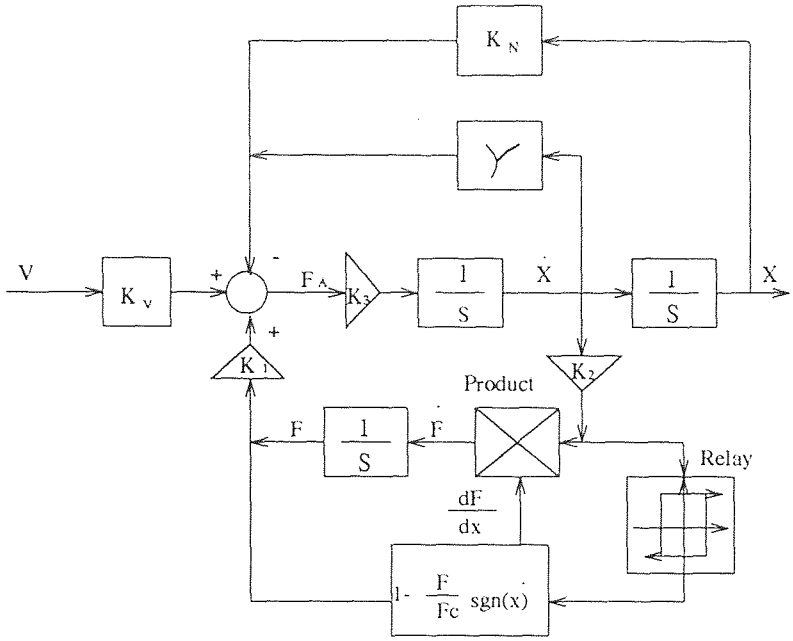

Figure 2.6 Simulation diagram of PZT stack

Furthermore, it has been found that two extra gain elements, K_1 the gain of $\dot{x}$ and K_2 the gain of F should be included to vary the effects of nonlinear force F as shown in Figure 2.6. For different kind of hysteresis loops the gain of $\dot{x}$ and F will be different, this will be easy to model different degrees of hysteresis. Another important additional feature is the relay block, it is introduced to get the correct $SGN(\dot{x})$ realization and to avoid undesirable rapid sign changes of $SGN(\dot{x})$ that may occur under the presence of some high frequency harmonic oscillation or noise. Such rapid chattering can significantly slow down the numerical simulation. The rationale of using a relay block is based on the observation that $SGN(\dot{x})$ only changes sign once when it crosses the line $\dot{x} = 0$ from $\dot{x} < 0$ to $\dot{x} > 0$ or from $\dot{x} > 0$ to $\dot{x} < 0$. The relay block solves this problem, since it considers not only the present input value but also the past input value. Within a small tolerance ϵ, it does not cause $SGN(\dot{x})$ to change sign. In later simulation ϵ is set to 10^{-4}.

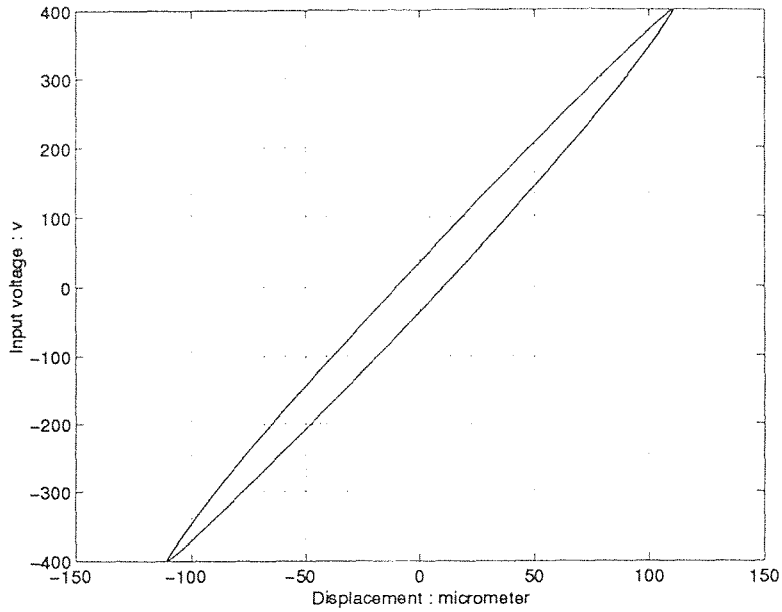

Figure 2.7 Hysteresis model for PZT stack $V = 400sin10t$

The properties of hysteresis loop are now assessed by numerical simulation. The input voltage (V) for the simulation is a low frequency sine wave $V = A\sin\omega t$ ($\omega = 1$ and 10, for different amplitude A). , with $K_N = 2.01944 \times 10^8$, $K = 5.8300$, $\gamma = 50000$, $K_1 = 200$, $K_2 = 10000$, $K_3 = 0.001$, $i = 0$ and $\sigma = 1$. Some simulation results are shown in Figures 2.7— 2.16.

The simulation results indicate while the amplitude of the input signal changes in two orders of magnitude, the characteristics of the spectral density of system output remains weakly invariant. Suppose the input signal has the frequency f, then there will be extra spectral components at $3f$, $5f$, $7f$ ...etc. due to the nonlinearity of the model. Define now h_1, h_3, h_5...etc. as the height in dB of spectral density at f, $3f$, $5f$...respectively. The harmonic ratios d_3, d_5, d_7...etc. can be defined as follows:

$$d_3 = h_3 - h_1 \quad dB \tag{2.12}$$

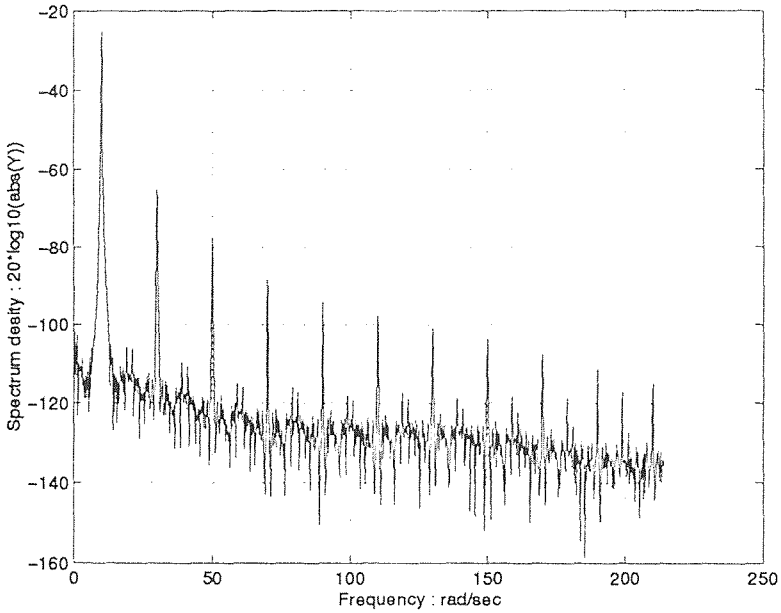

Figure 2.8 Spectral desity of hysteresis model for PZT stack $V = 400sin10t$

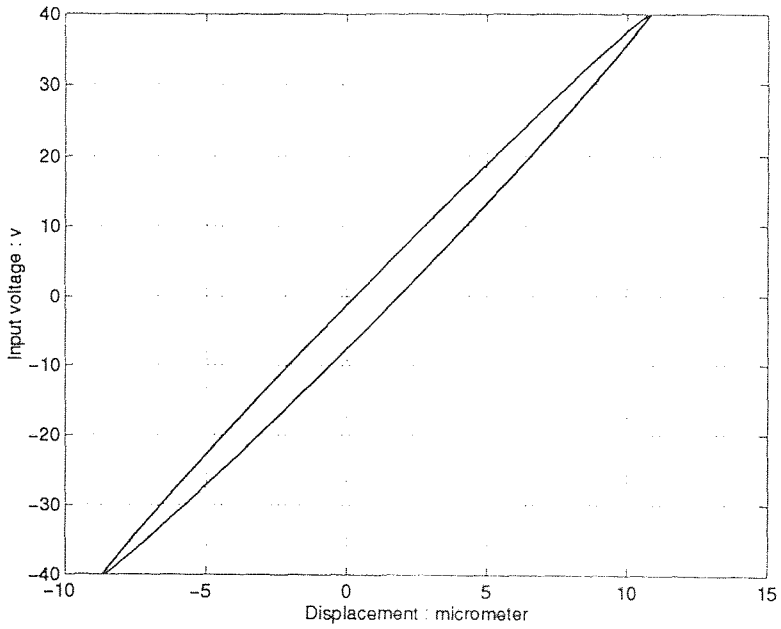

Figure 2.9 Hysteresis model for PZT stack $V = 40sin10t$

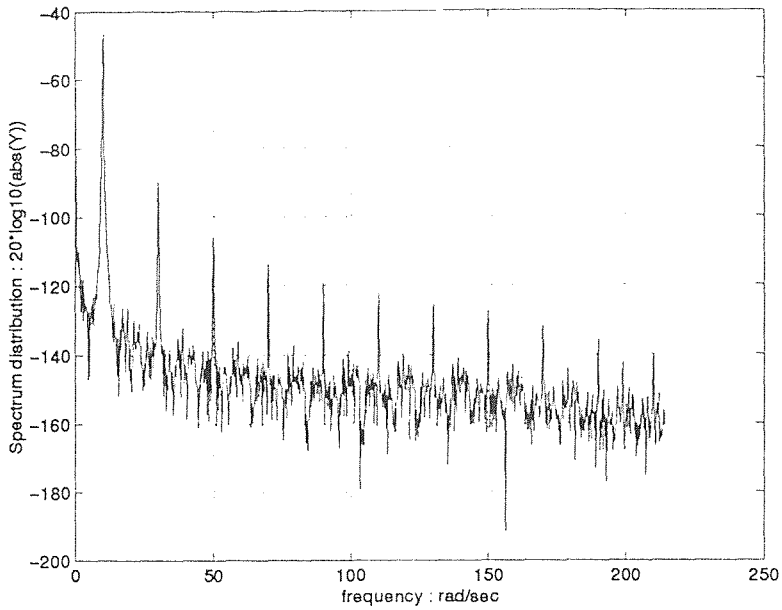

Figure 2.10 Spectral desity of hysteresis model for PZT stack $V = 40sin10t$

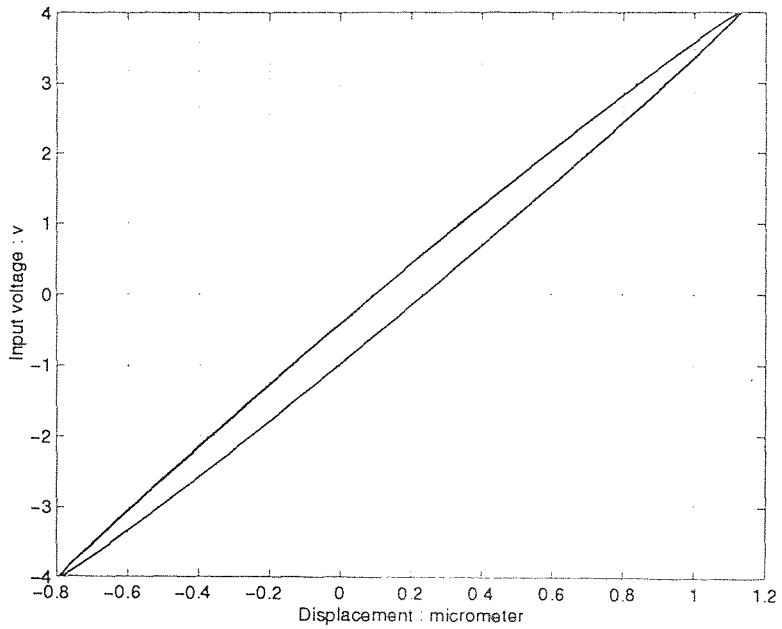

Figure 2.11 Hysteresis model for PZT stack $V = 4sin10t$

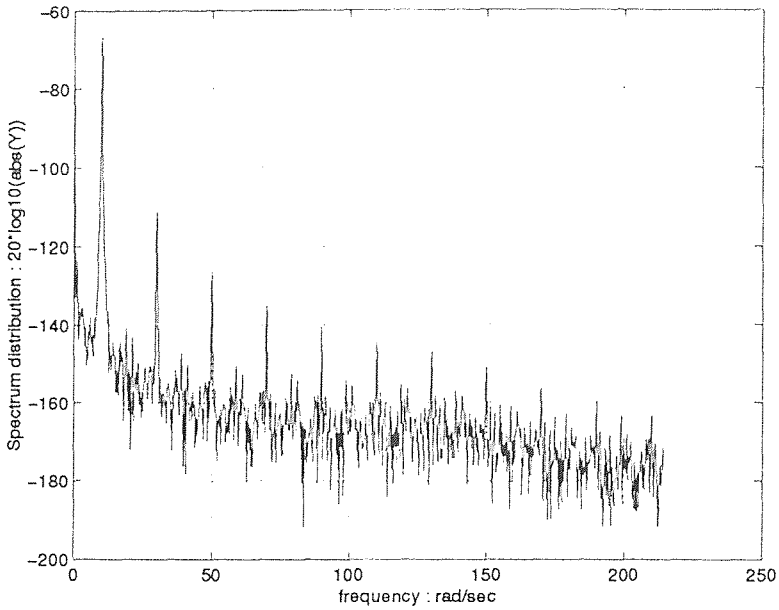

Figure 2.12 Spectral desity of hysteresis model for stack $V = 4sin10t$

$$d_5 = h_5 - h_3 \quad dB \tag{2.13}$$

$$d_7 = h_7 - h_5 \quad dB \tag{2.14}$$

...

When $V = 400 \sin 10t$,

$d_3 = -64dB - (-24dB) = -40dB$

$d_5 = -78dB - (-64dB) = -14dB$

$d_7 = -88dB - (-78dB) = -10dB$

...

For $V = 40 \sin 10t$,

$d_3 = -88dB - (-45dB) = -43dB$

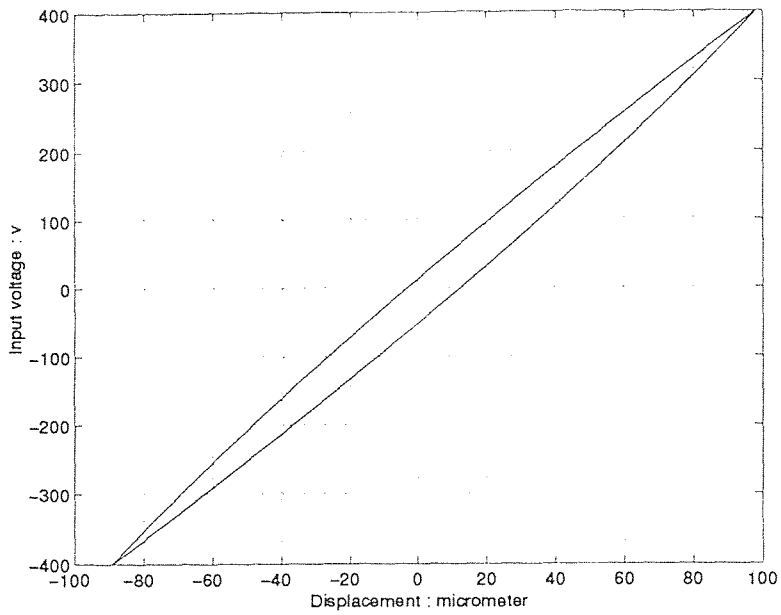

Figure 2.13 Hysteresis model for stack $V = 320sint$

$d_5 = -104dB - (-88)dB = -16dB$

$d_7 = -114dB - (-104)dB = -10dB$

...

For $V = 4\sin 10t$,

$d_3 = -111dB - (-66dB) = -45dB$

$d_5 = -127dB - (-111dB) = -16dB$

$d_7 = -127dB - (-137dB) = -10dB$

...

From the simulation data, it is found that as A ranges from one to six hundred, the variations in d_3, d_5, d_7 are bounded by $\pm 4dB$ as shown in Table 2.1. This means that this model is approximately scalable in this range, thus the term "weak scalability.".

When the input voltage is $A\sin t$, characteristics of the spectral density do not change, so this "weak scalability" is independent of input signal frequency. These

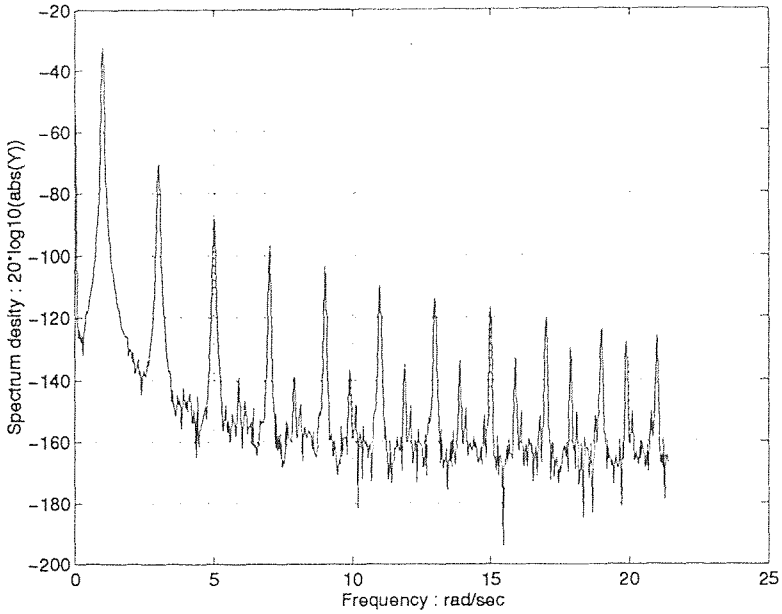

Figure 2.14 Spectral desity of hysteresis model for PZT stack $V = 320sint$

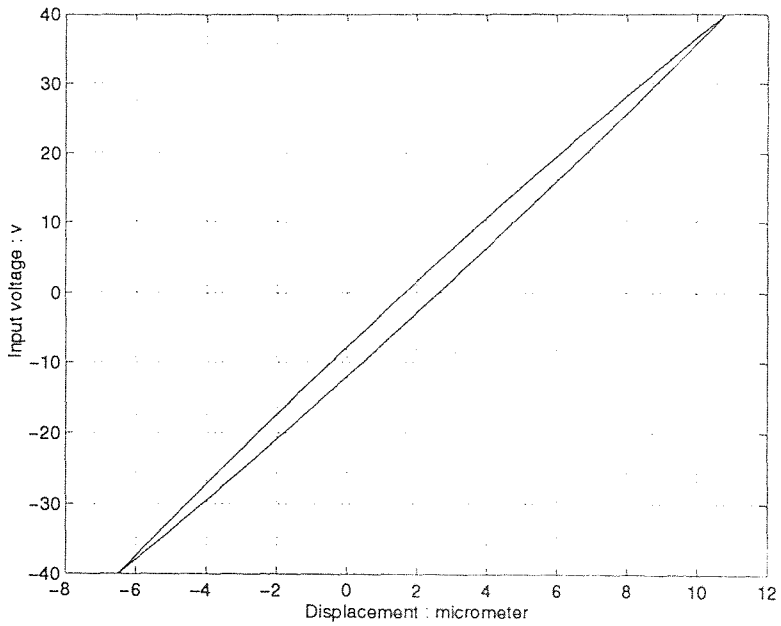

Figure 2.15 Hysteresis model for stack $V = 32sint$

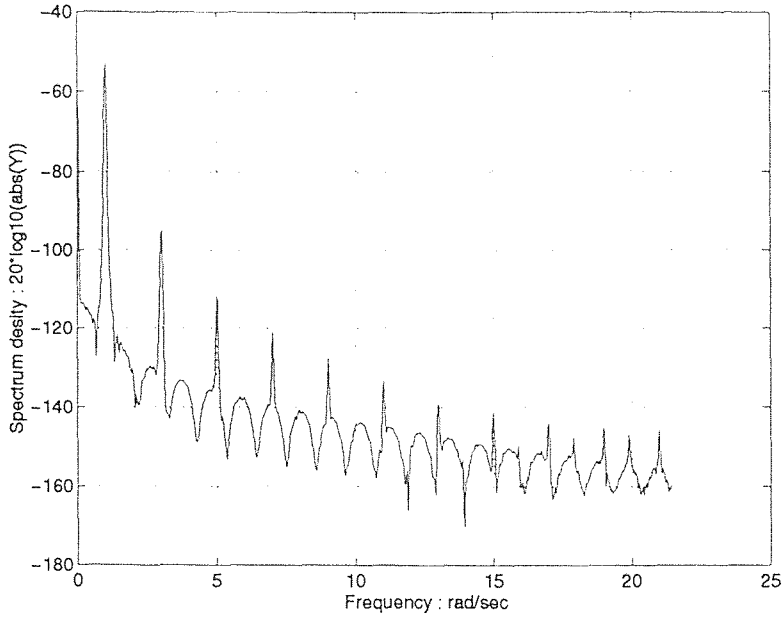

Figure 2.16 Spectral desity of hysteresis model for PZT stack $V = 32sint$

A	d_3	d_5	d_7
1	-46	-18	-7
4	-45	-16	-10
20	-46	-17	-9
40	-43	-16	-10
100	-40	-16	-10
200	-40	-15	-9
400	-40	-14	-10
600	-43	-10	-9

Table 2.1 Difference of spectral at $3f$, $5f$ and $7f$

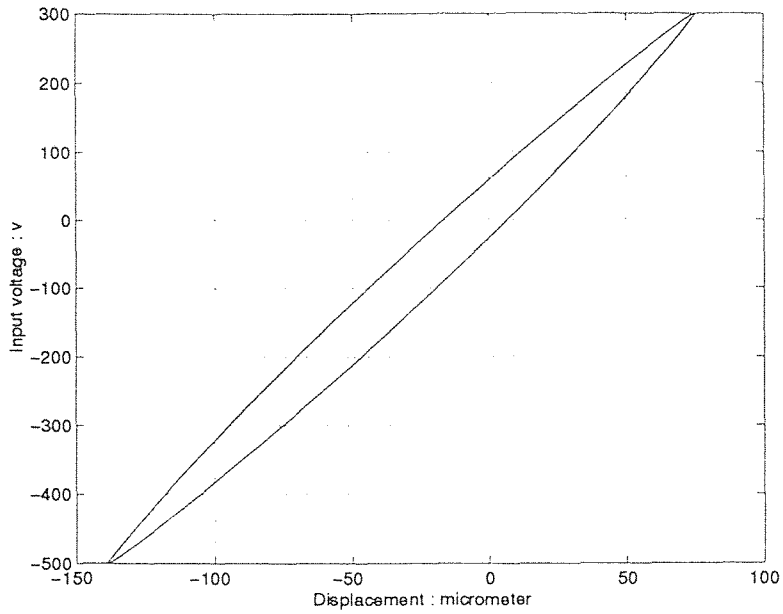

Figure 2.17 Hysteresis model for PZT stack $V = 400sin10t - 100$

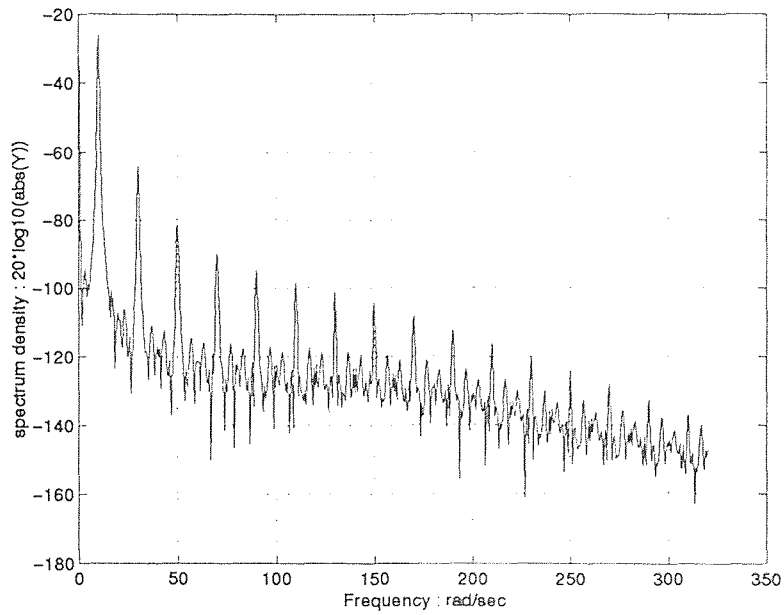

Figure 2.18: Spectral desity of hysteresis model for PZT stack $V = 400sin10t - 100$

simulation results together with their spectral analysis are shown in Figures 2.13—2.16

After extensive simulation, it is also found that when applied voltage has a DC offset, the characteristics of its spectral density does not change either. Since a DC signal can be considered as a signal with zero frequency, and this model has the property of frequency independent " weak scalability", therefore the DC offset will not affect the system's spectral power characteristics (compare Figure 2.8 with Figure 2.18) although the shape of hysteresis loop is changed (compare Figure 2.7 with Figure 2.17). The same model is simulated with two different input signals: (A) $V = 400 \sin 10t$; (B) $V = 400 \sin 10t - 100$. Simulation results are plotted in Figures 2.17—2.18.

2.2 Multi-loop Simulation

It is well known that PZT materials exhibit minor off-axis hysteresis loops inside the main hysteresis loop, as shown in Figure 2.19. A minor off-axis hysteresis loop may start from an arbitrary point on the curve of major hysteresis loop and terminate at the starting point. Suppose the biggest hysteresis loop in Figure 2.19 is loop1, middle one is loop2, smallest one is loop3. Then loop2 is minor loop of loop1, loop3 is minor loop of loop2.

Prandtl Laws[5] have been applied by Dahl[2] to account for the behavior of the minor loops with satisfactory results. These rules are now stated:

1) Immediately after the reversal of the sense of deformation, the slope of the stress-strain diagram has the same value as at the beginning of first loading.

2) The shape of any branch of the stress-strain diagram is uniquely determined by the position of the point where the last reversal of the sense of deformation occurred.

3) If the sense of deformation is not reversed again:

A) Any such branch will pass through the point where the last but one reversal of the sense of deformation occurred.

B) Thereafter, the stress-strain diagram continues as if the loop had never been formed.

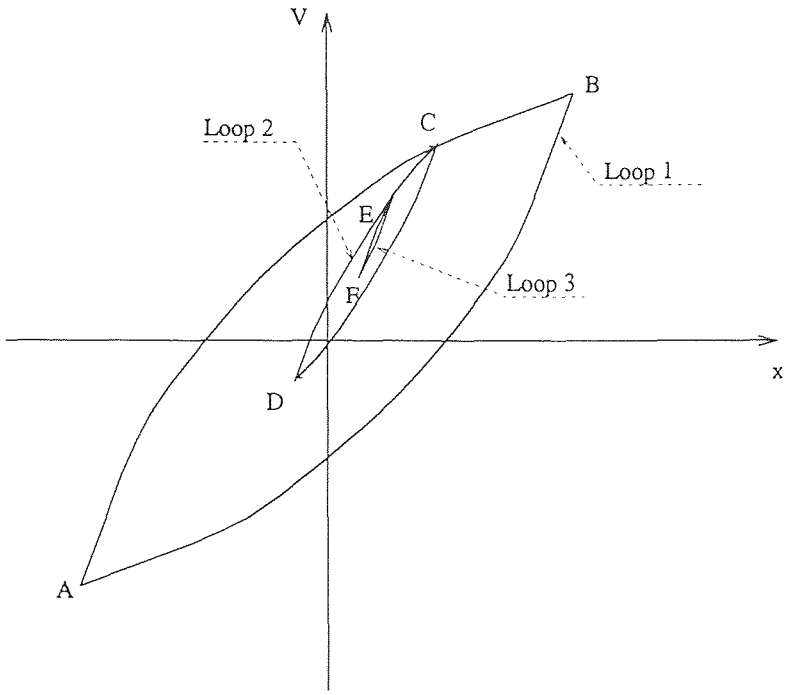

Figure 2.19 Example of minor hysteresis loop

Prandtl Laws clearly describe the characteristics of the off-axis minor hysteresis loops by means of a memory dependent algorithm. The simulation diagram is shown in Figure 2.20. It bears strong resemblance to the diagram for single loop simulation. However in this case, an extra block, a Matlab function MULTI.M is used. The codes of this function and the definition of those variables used in MULTI.M are given by Appendix A. A flowchart [2] corresponding to the nonlinear part of the PZT dynamics is given in Figure 2.21. It should be noted that $\dot{x}(N)$ represents the velocity at the step N for the numerical simulation.

For single loop situation, the SFM model is

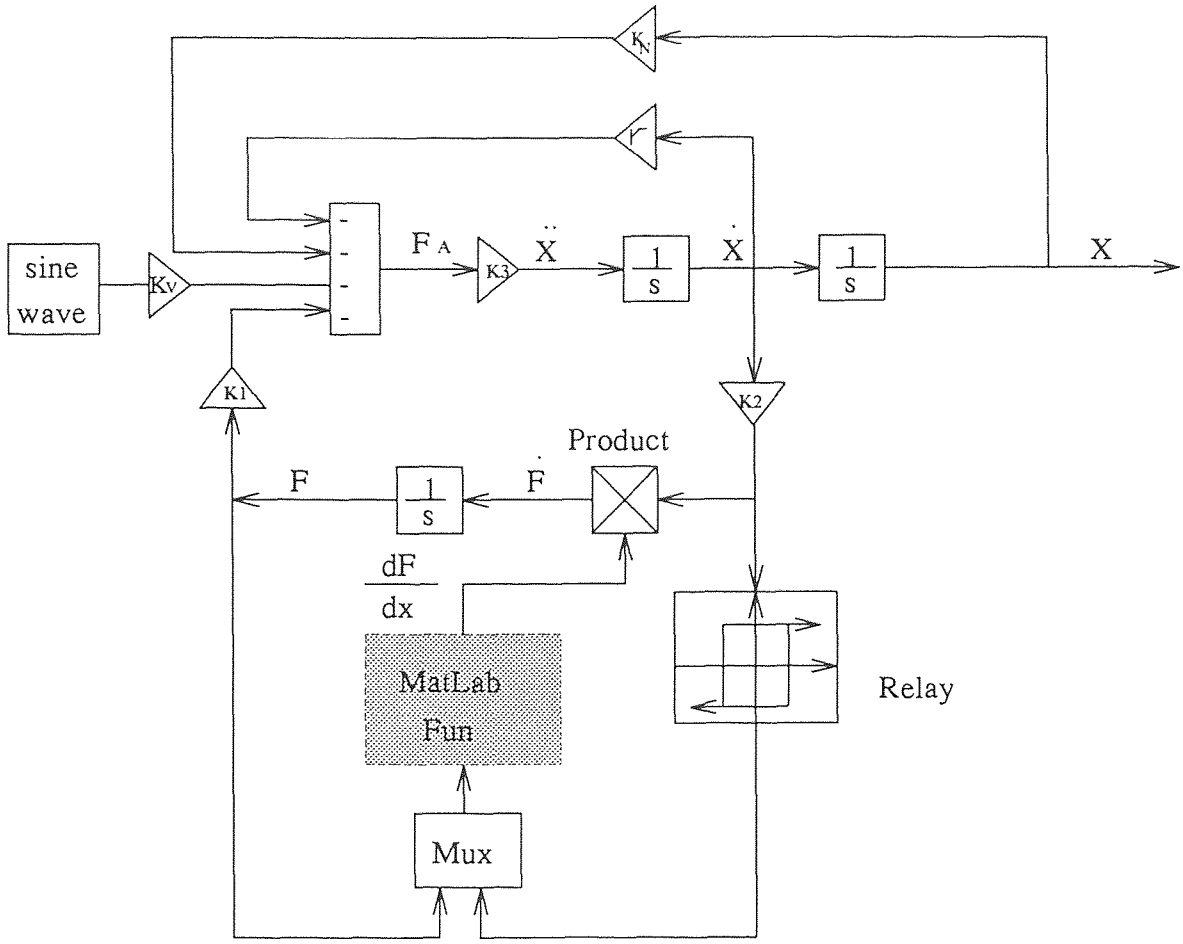

Figure 2.20 Simulation diagram for multiloop situation

$$\frac{dF}{dt} = \frac{dF}{dx}\frac{dx}{dt} \tag{2.15}$$

$$\frac{dF}{dx} = 1 - \frac{F}{F_c}SGN(\dot{x}) \tag{2.16}$$

It is clear that Prandtl Laws 1 is satisfied by (2.16) and to satisfy Prandtl Laws 3A, (2.16) is modified to [2]:

$$\frac{dF}{dx} = 2 - \frac{F - FEX(K)}{F_c}SGN(\dot{x}) \tag{2.17}$$

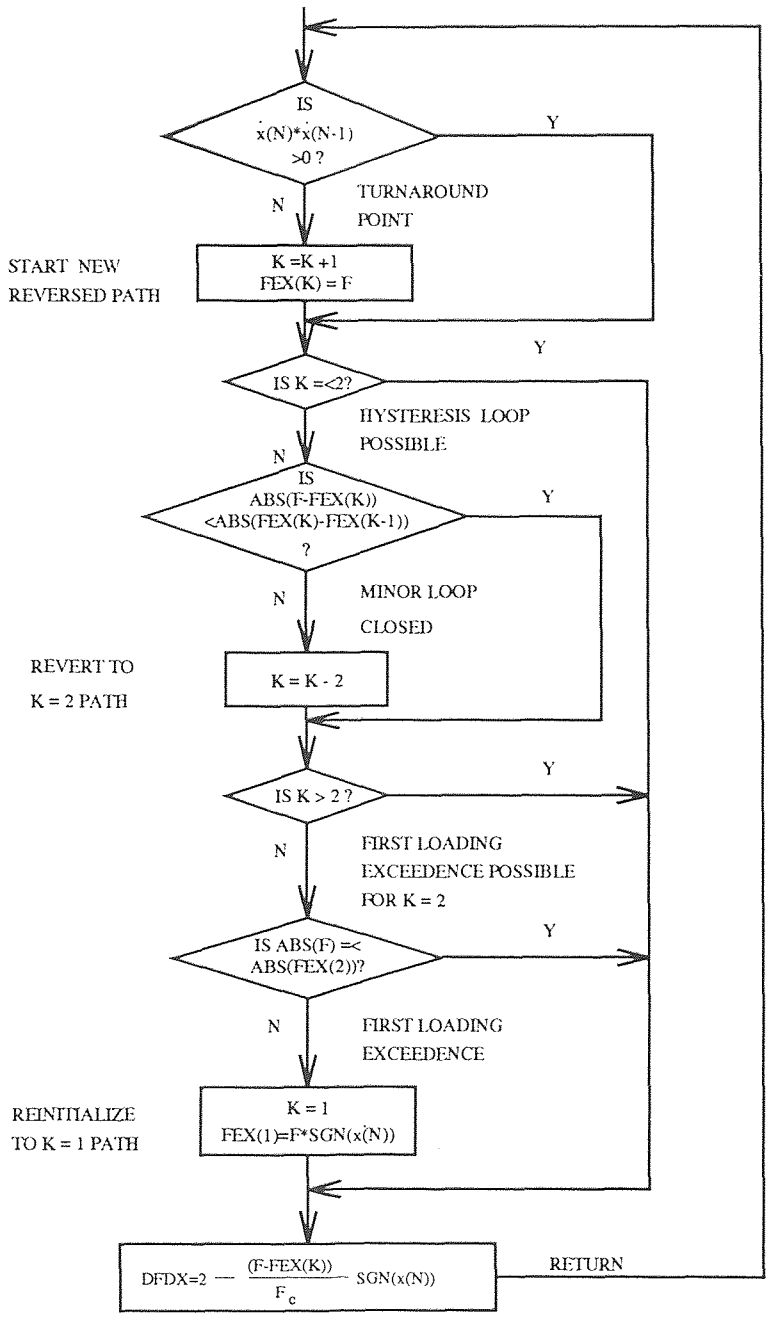

Figure 2.21 Flowchart of Matlab function MULTI.M

Where:

$K = K + 1$ is set at Kth turnaround point defined as $\dot{x}$ undergoes a sign change.

And

$FEX(K) = F$ is the hysteresis force at the time of Kth turnaround after K is set.

The initial conditions are:

$$K = 1 \tag{2.18}$$

$$FEX(1) = -F_c * SGN(\dot{x}(0)) \tag{2.19}$$

where F_c is the hysteresis force at the initial loading point. Since the initial curve is dependent on the past operating conditions, the previous values of K and $FEX(K)$, it is necessary to initialize the curve to be the first loading curve and hence $K = 1$ and the hysteresis force at the first loading point of the initial curve is set to $FEX(1)$. Substituting (2.19) into (2.17) once again provide (2.16) for single loop care. Therefore proper initialization requires running the simulation in the single configuration for "a while" and set $K = 1$ and F_c until the system output becomes stable.

Prandtl Law 3B is satisfied by the logic expression:

If

$$K > 2 \; AND \; |F - FEX(K)| \geq |FEX(K) - FEX(K-1)| \tag{2.20}$$

Then

$$K = K - 2 \tag{2.21}$$

For $K = 1$ or 2, there are at most two turnaround points, and hence only the major loop can exist. However for $K > 2$, there must be minor loops. Furthermore, if $FEX(K-1)$ is the hysteresis force at the point where minor loop starts and $FEX(K)$ is the hysteresis force at the point where the minor loop turnaround, then the difference between $FEX(K)$ and $FEX(K-1)$ is the maximum difference between any other two point on this minor loop. If logic equation (2.20) is satisfied, then the point which has the hysteresis force F returns to the point where minor loop originated, namely minor loop closed and the subsequent curve will become the $K-2$ loading curve as if the minor loop was never formed.

Another problem that can arise is the following:

When $K = 1$ or larger than 2, the solid friction model does not present unrealistic behavior. However, if $K = 2$ and the branch keeps going without turnaround, then finally it will reaches a point which has the hysteresis force F that $|F| \geq |FEX(2)|$, then the $K = 1$ initial condition or maximum value in its previous history of first loading curve will be exceeded. If a new $FEX(1)$ is not set at this moment, and if $K = 2$ curve continued without a velocity reversal or turnaround, then the $K = 2$ branch will finally cross the constant line $F_c * SGN(\dot{x}(0))$. This is intuitively incorrect behavior for most hysteresis phenomena. To avoid such unrealistic situation, an F_c limiting logic is introduced:

If $K = 2$ and $|F| \geq F_c$

then $K = 1$ and $FEX(1) = -F_c * SGN(\dot{x})$

Equally, this correction can be made at the first loading exceedance, i.e.

If $K = 2$ and $|F| \geq |FEX(2)|$

Then $K = 1$ and $FEX(1) = F_c * SGN(\dot{x})$

Because of this limiting logic there will be a discontinuity in dF/dx at the first loading exceedance point, and the curve of $K = 2$ becomes a new $K = 1$ curve and then the new $K = 1$ curve will be approximate to the original $K = 1$ curve.

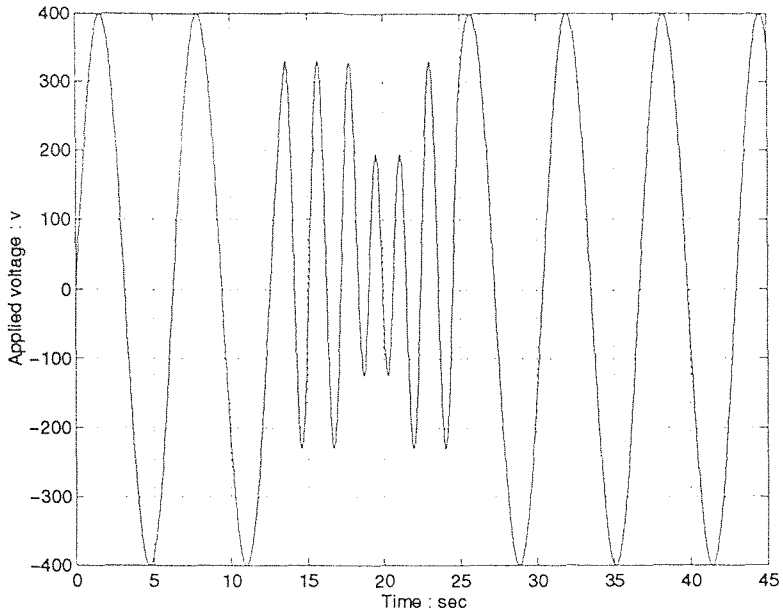

Figure 2.22 Input signal for multiloop simulation

For $K_N = 2.0944 \times 10^8$, $K_V = 5.8300$, $\gamma = 50000$ $K_1 = 500$, $K_2 = 10000$, $K_3 = 0.001$, $i = 0$ and $\sigma = 5$, the simulation results are plotted in Figure 2.23 and Figure 2.24.

The applied voltage is a combination of $400sint$, $280sin3t$, $160sin4t$ as shown in Figure 2.22. Therefore there are 3 loops. The biggest one is, by definition, major hysteresis loop, the rest are considered as minor hysteresis loops. Denote the middle one minor loop 1 and the smallest one minor loop 2. Major hysteresis loop starts from point A, along with curve 1, now the loop index $K = 1$. When it reaches turnaround point B, it follows the curve 2 which is symmetrical to curve 1, the virgin curve with respect to the origin (Prandtl Laws 2). The loop index is now incremented to 2. Because of the symmetry, the slope at point A along curve 1 is the same as that at point B along curve 2(Prandtl Laws 1). Curve 2 will finally reach point A again, then turnaround and follow curve 1 again(Prandtl Laws 3A). Next time when it reaches point C, the applied voltage changes its direction, so the curve turnaround at point C, and along with curve 3, $K = 2$. The slope(m_C) at point C along curve 3 is the

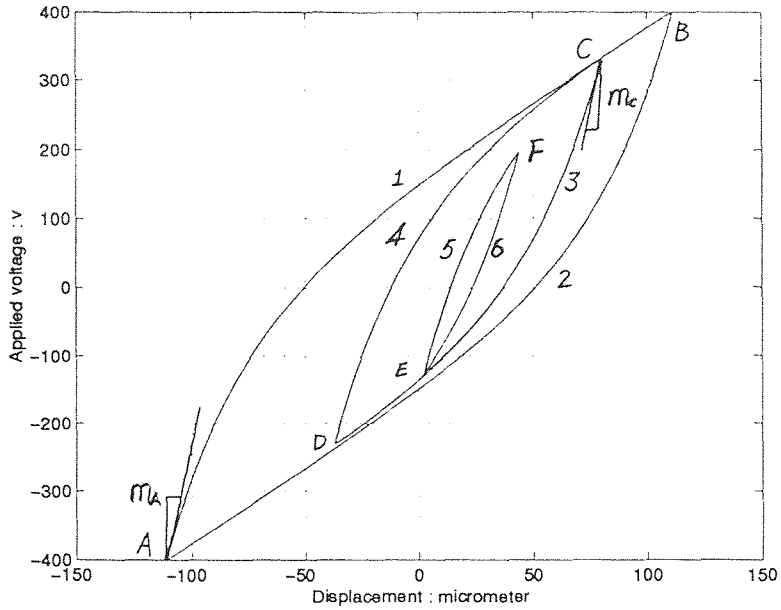

Figure 2.23 Simulation result of hysteresis model for PZT stack

same as that (m_A, see Figure 2.23) at point A along with curve 1 (Prandtl Laws 2). Then after it turnaround at point D, it follows the curve 4, $K = 3$, and reach point C again(Prandtl Laws 3A). So curve 3 and curve 4 formed a minor hysteresis loop(minor loop 1). When it reaches point C again, the loop index K reset to 1. Since point C both belong to major loop and minor loop 1, so at that moment minor loop 1 is closed, it return to curve 1 as if minor loop1 was never formed (Prandtl Laws 3B). Similarly for minor loop 2, minor loop 1 is its major hysteresis loop as if the major loop does not exist. The only difference is that for minor loop 1 the loop index $K = 2$ or 3, but for minor loop 2, $K = 3$ or 4.

In Figure 2.24, the applied voltage is the same as that before except a DC offset -100 is added to the applied voltage. The shape of the hysteresis loops is changed due to a DC offset, but their spectral characteristics do not change. And all loops still follow Prandtl Laws as well as that in Figure 2.23.

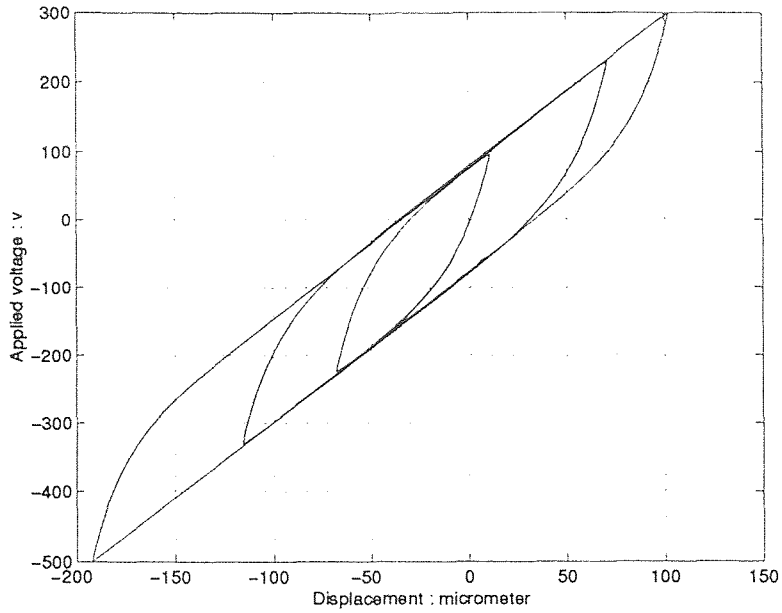

Figure 2.24 Simulation result of PZT model when input have a DC offset

2.3 Model for Actual Experimental Date

The experimental data in Dahl's [2] are used to parameterized the model by adjusting σ, i, γ, K_1 and K_2. Since the values of σ and i are already known, it remains to determine K_1, K_2, K_V, K_N and γ as follows:

$$K_V = \frac{NA(1+b)d_{33}}{HS_{33}} \approx 5.8300 \quad N/V \tag{2.22}$$

$$K_N = \frac{A}{HS_{33}} \approx 2.01944 \times 10^8 \quad N/m \tag{2.23}$$

γ is a damping coefficient. Its presence is due to mechanical losses in the PZT materials and it has the effect of stabilizing the system. The value of γ is, in general, unknown. It was found by simulation that $\gamma \approx 5 \times 10^4$ is appropriate. Other parameters are also adjusted to match the experimental data. The parameters are chosen for the simulation model:

$K_N = 2.01944 \times 10^8$

Point	Voltage	S	D	e	a
A	-160	-24.76	-23.98	-0.78	3.25 %
B	-100	-17.49	-18.05	-0.54	2.92 %
C	-50	-11.00	-10.05	-0.95	9.55 %
D	0	-3.34	-3.19	-0.15	4.70 %
E	50	+4.98	+5.03	-0.05	0.99 %
F	100	+14.66	+14.61	+0.05	0.34 %
G	150	+25.08	+25.58	-0.50	1.95 %
H	200	+36.14	+37.68	+1.54	4.09 %
I	250	+48.29	+48.88	-0.59	1.21 %
J	290	+58.83	+60.07	-1.24	2.06 %

Table 2.2 Comparation of simulation data and experiment data

$K = 5.8300$

$\gamma = 50000$

$K_1 = 500$

$K_2 = 10000$

$K_3 = 0.001$

$\sigma = 3.2$

$i = 0$

When modeling PZT stack with Dahl's experiment data, the most important thing is to fit the first loading curve because all the following curves are based on the first loading curve. Therefore emphasis is placed on the first loading curve of both simulation and experiment result. As show in Figure 2.25, the first loading curve is curve AHJ. The result of comparison is shown in Table 2.2. Where S(micrometer) represents Simulation data, D(micrometer) represents experiment data. $e = S - D$ is the difference between simulation data and experiment data. $a = 100 \times \left|\frac{e}{D}\right| \%$ is the percentage of difference compare to experimental data.

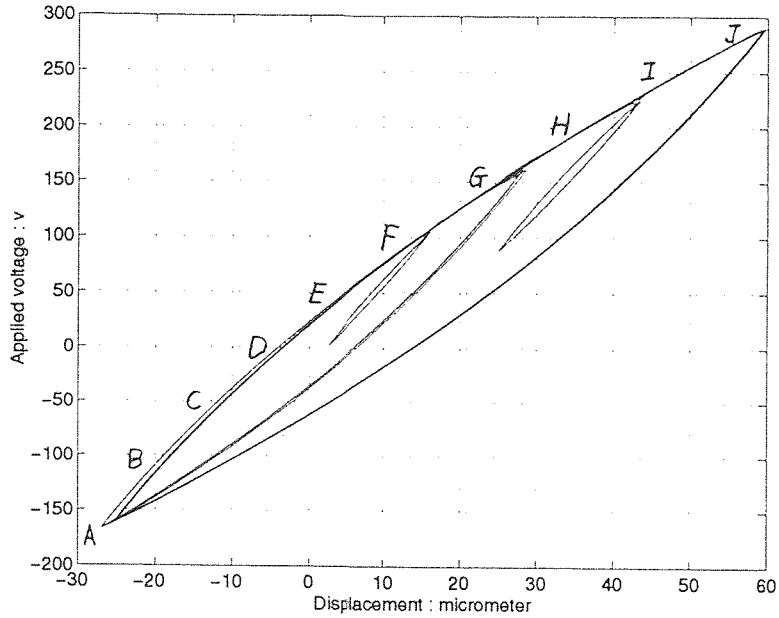

Figure 2.25 Simulation result of PZT stack model for experimental data

CHAPTER 3

CONTROL OF PZT STACK

3.1 Measure of Nonlinearity

3.1.1 Measure from I/O Curve

A simple and intuitive way to measure nonlinear distortion of hysteresis loop is to calculate the area of the hysteresis loop formed between the input and output. Suppose the hysteresis loop in Figure 3.1 has area S_A, and suppose with the same input signal the I/O curve of another system(System B) has the area S_B, where $S_B > S_A$, then it is concluded that the nonlinearity of System B is more severe than that of System A.

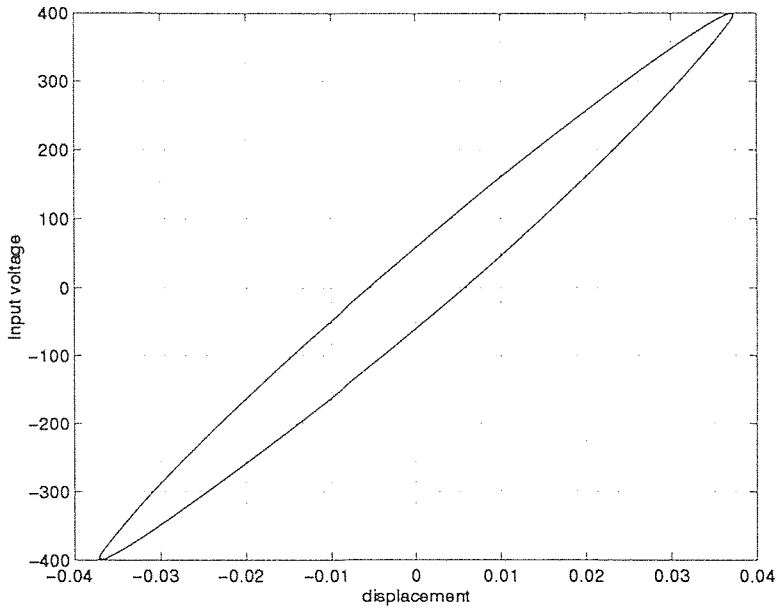

Figure 3.1 Nonliear hysteresis loop of System A

However, such measure has its drawbacks. For example, consider the following linear transfer function(System C):

$$T(s) = \frac{1}{s^2 + 100s + 10000} \tag{3.1}$$

When the same signal is applied to the model, we can find its Lissajous's pattern is almost the same as the hysteresis loop in Figure 3.1, as shown in Figure 3.2.

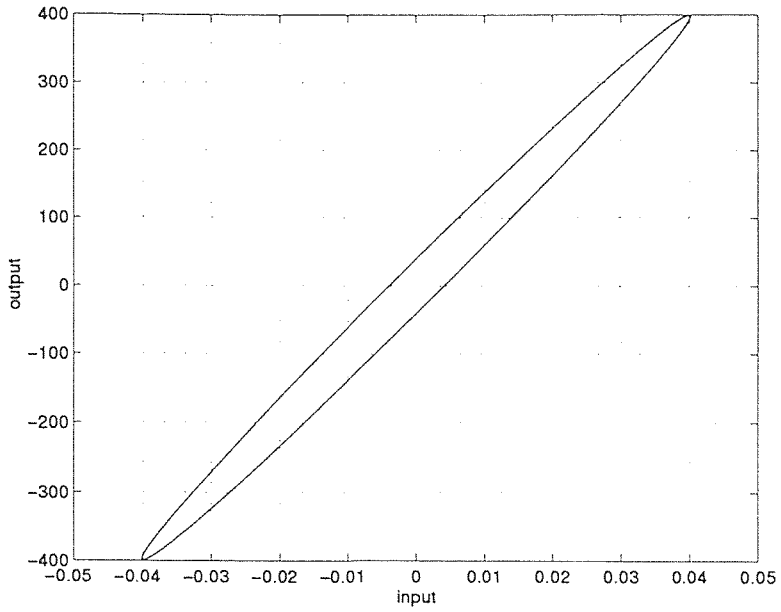

Figure 3.2 I/O curve of System C

So an alternative way to measure nonlinearity is now proposed.

3.1.2 Probing Signal Spectral Density

Another method to measure nonlinearity is to analyze the distortion spectrum by means of Fast Fourier Transform(FFT).

For a linear system the characteristics of the spectral density of its input and output are the same, but for nonlinear system they are different. For example, in Figure 3.1 and Figure 3.2, although the shape of both loops is similar, when use

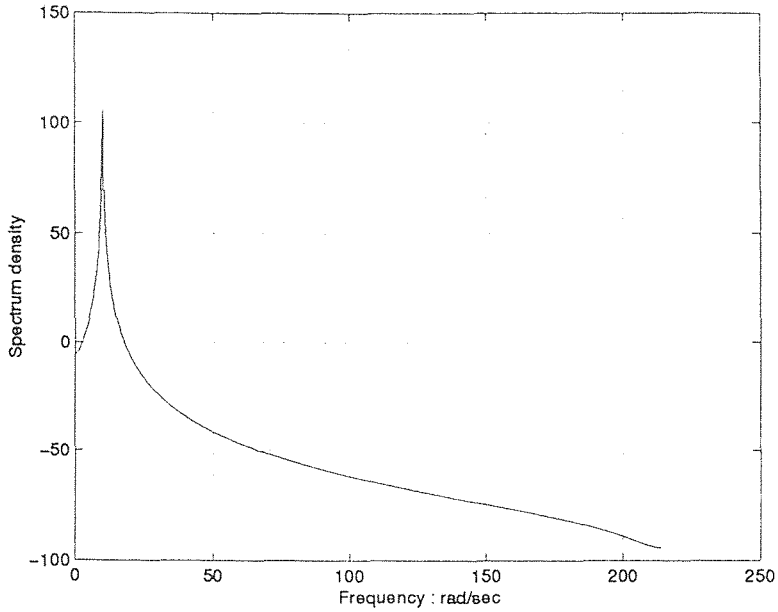

Figure 3.3 Spectral density of $Asin10t$

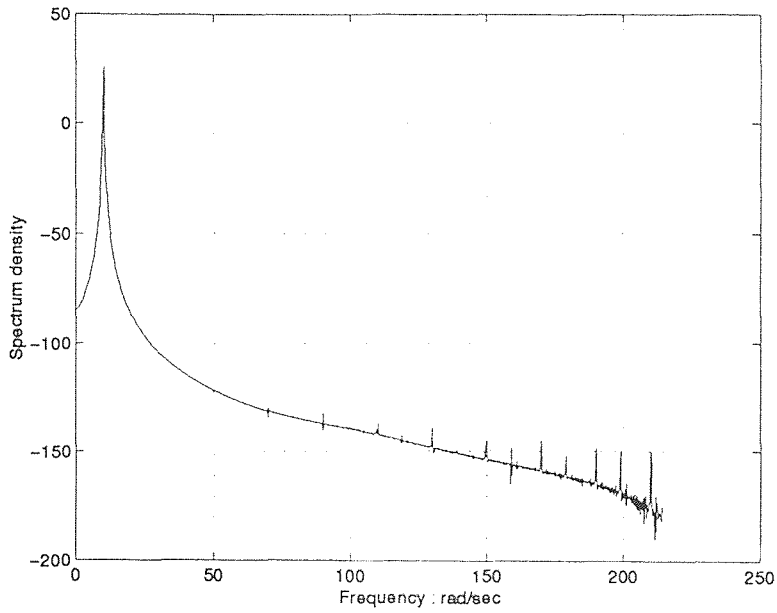

Figure 3.4 Spectral density of System C

FFT to calculate the spectral density of them, it is found that their spectral density distribution are totally different, see Figures 3.3—3.5.

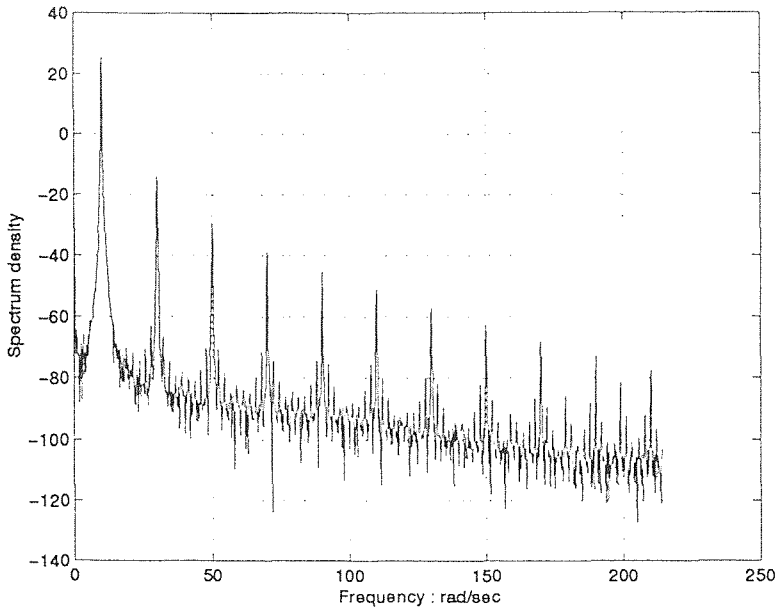

Figure 3.5 Spectral density of System A

By comparing Figure 3.3 with Figure 3.4, it is clear that for a linear system the characteristics of spectral density of its input and output are the same(the high frequency components in Figure 3.4 are due to numerical effects and are at least 150dB lower than that of signal frequency). Further comparison between Figure 3.3 and Figure 3.5 reveals that for a nonlinear system the characteristics of spectral density of its input and output are totally different, besides the fundamental harmonic, there are extra harmonic components. Suppose the frequency of the input signal is f, then due to the hysteresis nonlinearity, there are extra components appearing at $3f$, $5f$, $7f$ ... etc. The magnitude of these higher order harmonics is a direct indication of the nonlinearity of the system. Therefore, spectral analysis is a viable way to measure the nonlinearity.

3.2 Dither Function

A dither is a high frequency signal introduced into a nonlinear system in order to improve its performance. By sweeping back and forth quickly across the domain of a nonlinear element, a dither has the effect of averaging the nonlinearity and making it smoother, and in some sense reduced the nonlinearity of the system. If the frequency of dither is high enough, it is easy to get filtered out before it reaches the output. As previously discussed in Chapter 1, adding a dither and a low pass filter to a nonlinear system, it becomes a system shown in Figure 1.2. Thereafter, even though the nonlinear element still exists, the output of the system is "linear" to its input.

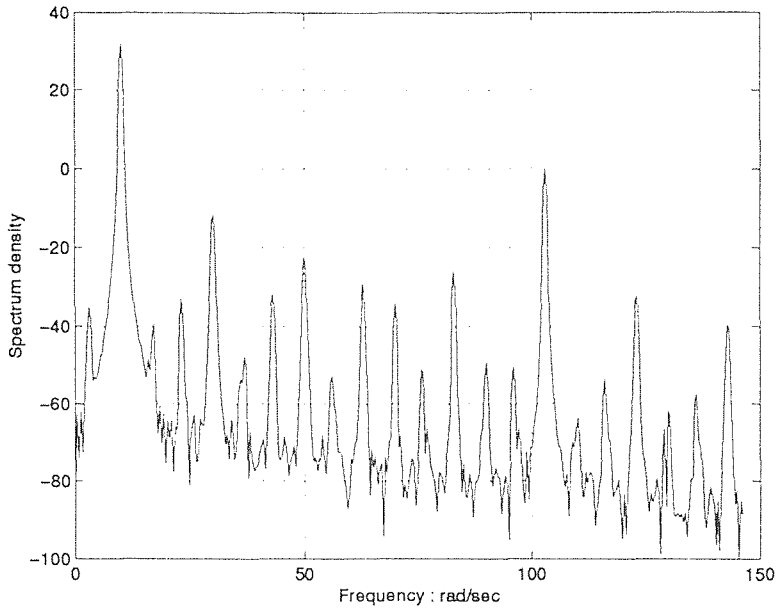

Figure 3.6 Spectral density of model of PZT stack while $A = 10$

A comparison on some simulation results is now made to access dither affects on a nonlinear system. Apply now a low frequency sine wave($400sin10t$) to the model of PZT stack actuator, the spectral distribution of its output is shown in Figure 3.5. A dither($Asin103t$) is then injected to the system. For different dither amplitude A, the spectral distribution of system output is shown in Figures 3.6—3.8.

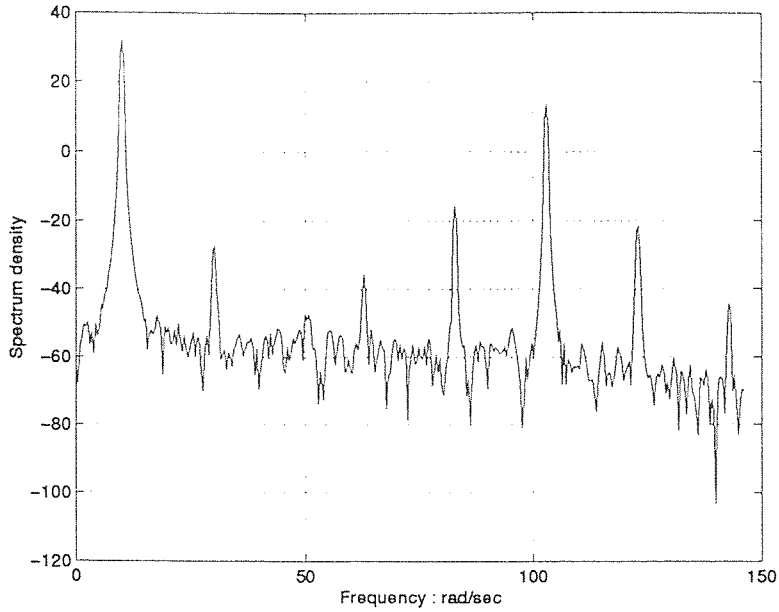

Figure 3.7 Spectral density of model of PZT stack while $A = 50$

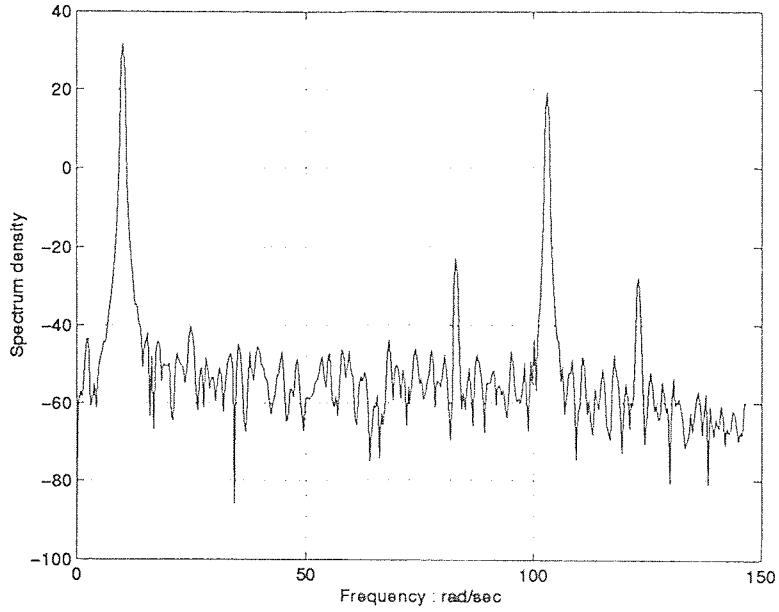

Figure 3.8 Spectral density of model of PZT stack while $A = 100$

From Figure 3.5, it is observed that when the frequency of input signal is f, the spectral of nonlinear element appears at the odd harmonics with decreasing strength. After the dither is introduced, the spectral power of the higher order harmonic decreases as the amplitude of dither increases. Suppose that the height of spectral at $(2n+1)f$ is given by $H_{(2n+1)f}$, $n = 0, 1, 2 \cdots$. ($H_{(2n+1)f}$ expressed as dimensionless quantities), the following ratios are now defined:

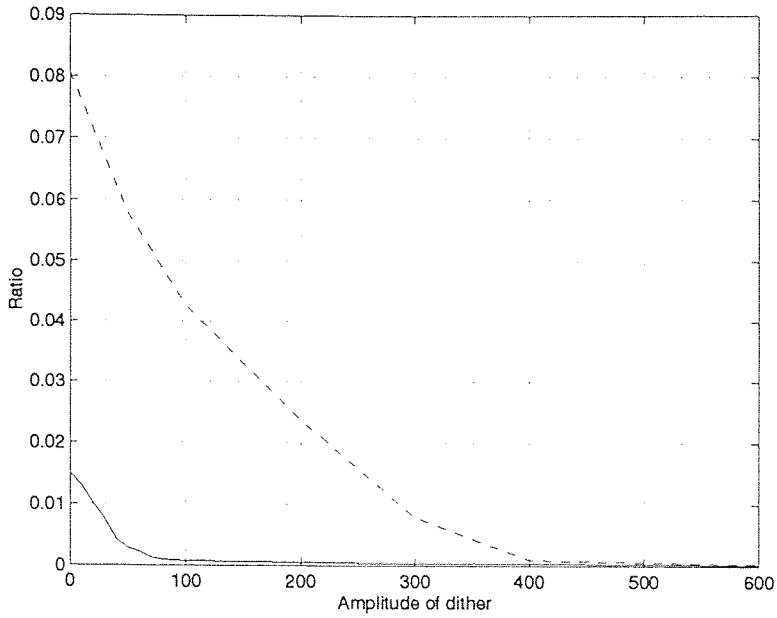

Figure 3.9 Relation between ratio and amplitude of dither

$$r_3 = \frac{H_{3f}}{H_f} \tag{3.2}$$

$$r_5 = \frac{H_{5f}}{H_f} \tag{3.3}$$

$$r_7 = \frac{H_{7f}}{H_f} \tag{3.4}$$

...

Furthermore, define the system harmonic ratio as:

$$\overline{r} = \frac{(r_3 + r_5 + r_7)}{3} = \frac{H_{3f} + H_{5f} + H_{7f}}{3H_f} \tag{3.5}$$

Since r_9, $r_{11} \cdots$ is relatively small compare to r_3, r_5, r_7, emphasis is placed on r_3, r_5, r_7 only. After extensive simulation, it is found that as the dither amplitude increases, the ratio of spectrum decreases. Refer to Figure 3.9, the value in y-axis is the average value of r_3, r_5, r_7. The x-axis represent the amplitude of dither. Here two model with different degree of nonlinearity are compared. All the parameters in these two models are same as those in page 11 except for K_1, the gain of F. The results are summarized in Figure 3.9, dashed line is for $K_1 = 200$ and solid line is for $K_1 = 2000$. It is observed that, as the nonlinearity is increased, proportionally higher dither amplitude is required to achieve the same harmonic ratio.

3.3 Harmonic Contents Attenuation

Although nonlinearity smoothing by dither is the objective of this work, issues such as "what is a suitable dither?" and "what is a criterion of reduction of nonlinearity?" remain to be addressed. As discussed in Section 3.2, a dither has the effect of averaging the nonlinearity of the PZT stack system, i.e. attenuating the harmonic components $H_{(2n+1)f}$, $n = 1, 2, 3 \cdots$. However, to completely recover the linearity, unacceptably large dither is required. Therefore, it is desirable to balance the amplitude against linearity recovery. This observation motivates the definition of a suitable dither amplitude as the minimum dither amplitude so that the system harmonic ratio $\overline{r}$ (3.5) is less than a prespecified value.

For example, as shown in Figure 3.9, $\overline{r}$ of original nonlinear system (dashed line) is 0.08061, and if it is to be reduce by $40dB(\overline{r} = 0.0008061)$, then adding a dither with $A \approx 400$, meets the requirement. Since the PZT model is "weak scalable", its distortion spectrum is relatively invariant. Therefore $\overline{r}$ is used as a

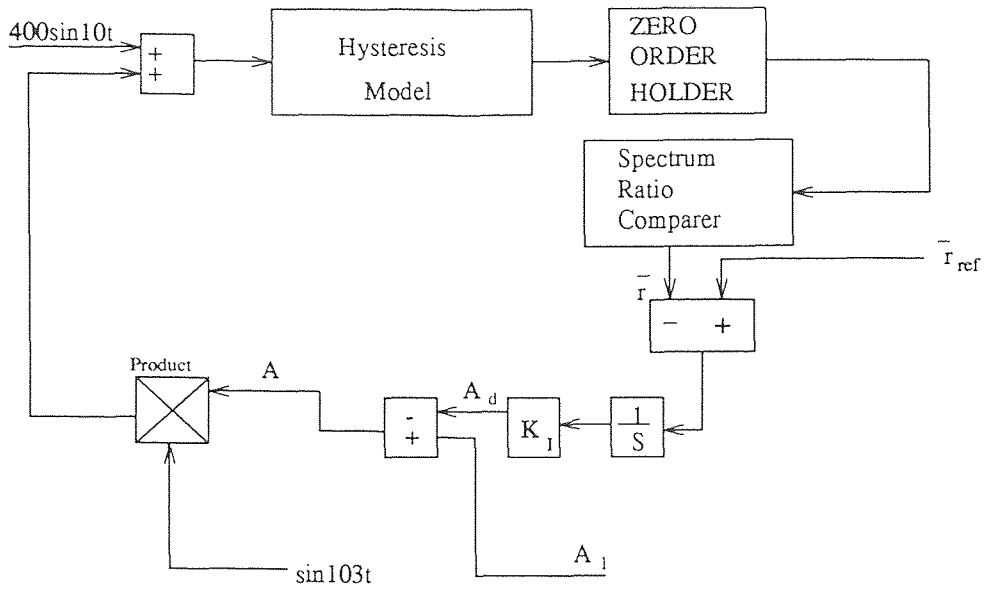

Figure 3.10 System with integral controller and ratio comparator

criterion in harmonic analysis to measure nonlinearity and later as a basis adaptive dither control.

The reason for considering adaptive dither control, where the suitable dither amplitude is automatically generated, is that for most systems, such amplitude is unknown on a priori basis. The adaptive mechanism is based on the following:

First, an arbitrarily small value dither amplitude is chosen. Secondly, $\overline{r}$ is calculated by real-time FFT. Thirdly, an error signal $e = \overline{r}_{ref} - \overline{r}$ is formed where $\overline{r}_{ref}$ is prespecified. Finally the dither amplitude A is continuously adjusted by a integral controller that operate on the error signal:

$$e = \overline{r}_{ref} - \overline{r} \tag{3.6}$$

$$A_d = K_I \int_0^t e(\tau) d\tau \tag{3.7}$$

$$A = A_1 - A_d \tag{3.8}$$

Upon adding the integral controller and the ratio comparator to the PZT model, the adaptive closed loop system is shown in Figure 3.10. The spectrum comparator

calculate $\overline{r} = \dfrac{H_{3f} + H_{5f} + H_{7f}}{3H_f}$ every 512 sample points. It is realized by a Matlab function S_COM.M(program list is on appendix A).

3.4 Simulation Result

Simulation studies are now carried out using the hysteresis model with the parameters given in page 11. As shown in Figure 3.10, the amplitude of the dither is $A = A_1 - A_d$, where A_1 is the initial best estimate of the suitable dither amplitude and A_d is the compensatory dither amplitude generated by the adaptive mechanism. $\overline{r}$ (3.5) is the output of spectrum ratio comparator and e (3.6) is error between the reference signal $\overline{r}_{ref}$ and $\overline{r}$. Moreover, x is PZT end displacement, while x_l is the baseband version of x. From Figure 3.9, in an undithered system $\overline{r} = 0.0149$ ($K_1 = 200$), suppose that $\overline{r}_{ref=}0.001$. The system shown in Figure 3.10 is simulated with $K_I = 1000$, $A_1 = 20(5\%a)$ and input signal is $400sin10t$. The simulation result is show in Figures 3.12 and 3.11. It shows finally when the amplitude of dither is $20 - (-45) = 65$. it meets the distortion requirement $\overline{r}_{ref}$.

In fact the phase of dither is not important, so that $a \sin w_d t$ has the same effects as $a \sin(w_d t + \pi) = -a \sin w_d t$. This can be verified by simulating the system again with all the same parameters used before except $K_I = -1000$. The simulation result is show in Figure 3.13 and Figure 3.14. It shows finally the suitable dither amplitude becomes $20 - (+85) = -65$. This shows the whole system is quite robust and it is insensitive to the sign of gain of integral controller.

The spectral density of x and x_l is shown in Figure 3.15 and 3.16, it shows the spectral density of x_l has almost the same characteristics as that of the input (the harmonic components in Figure 3.16 are due to numerical effects. and the filter used here is a fourth order butterworth low pass filter with cut-off frequency 20 rad/sec) i.e. x_l is "linear" to the input ($asin10t$).

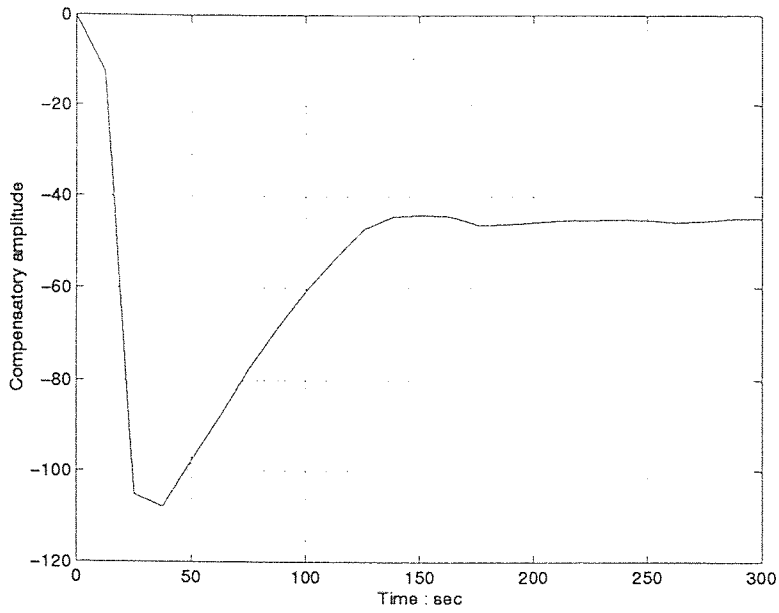

Figure 3.11 Compensatory dither amplitude when $K_I = 1000$

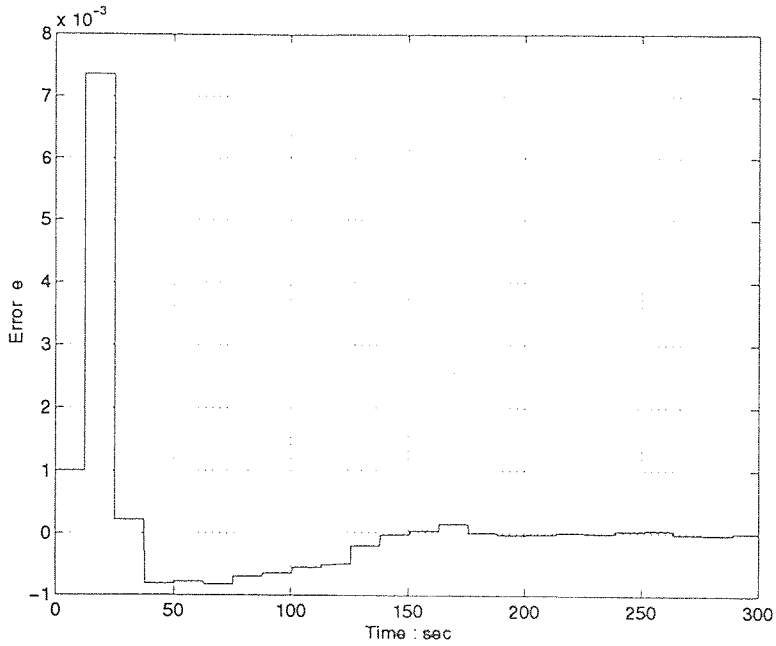

Figure 3.12 Error signal in integral control when $K_I = 1000$

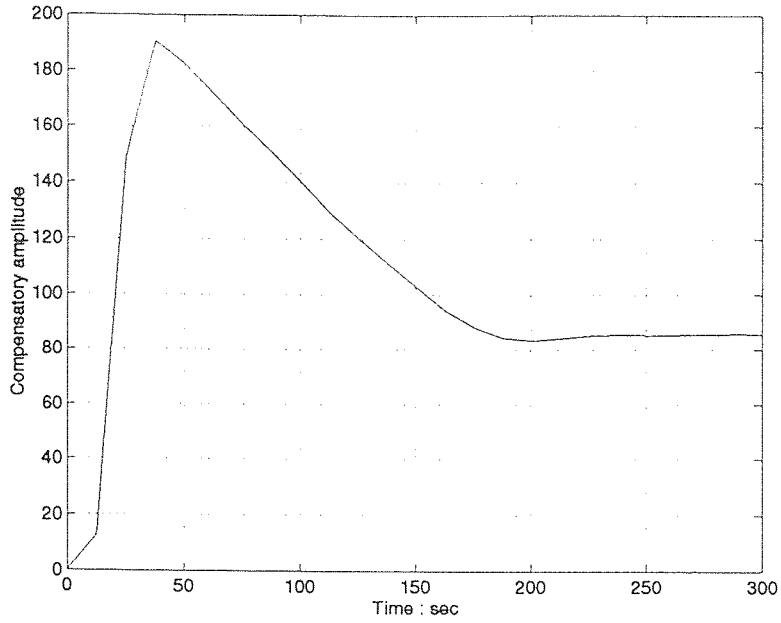

Figure 3.13 Compensatory dither amplitude when $K_I = -1000$

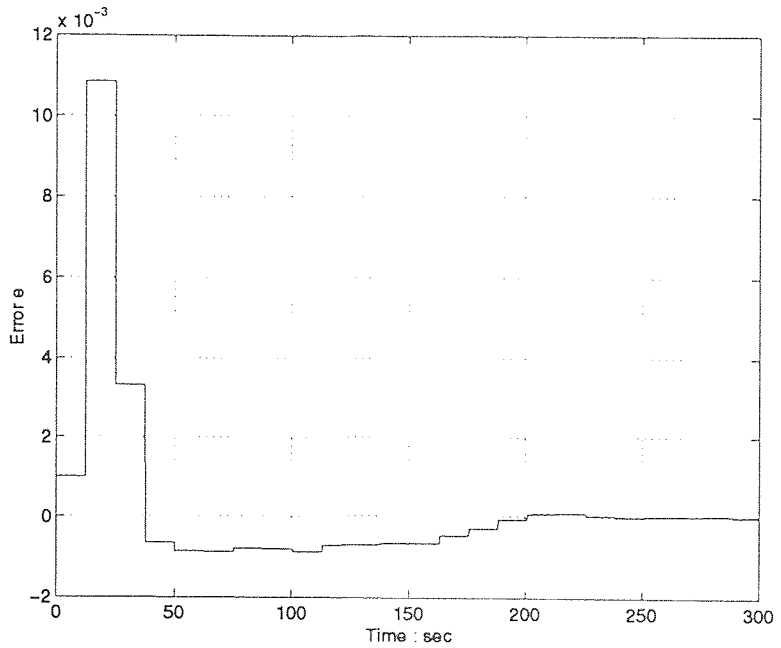

Figure 3.14 Error signal in integral control when $K_I = -1000$

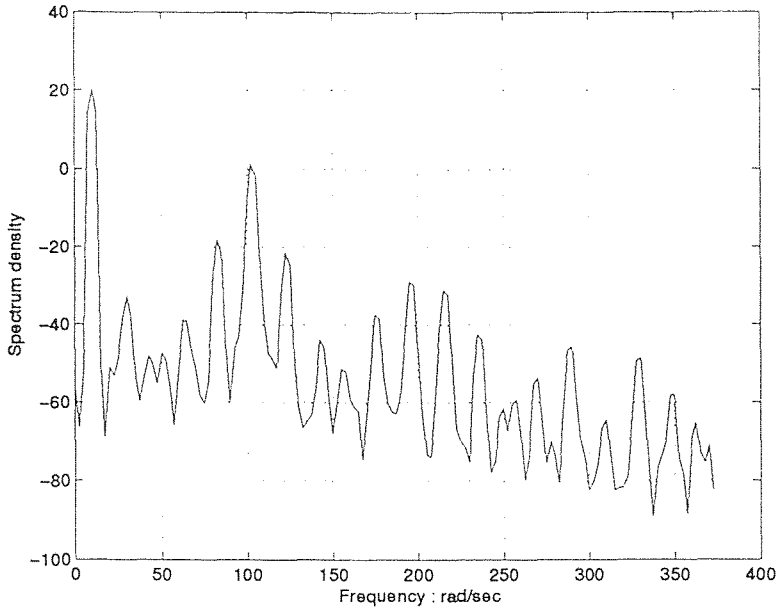

Figure 3.15 Spectral density of displacement x

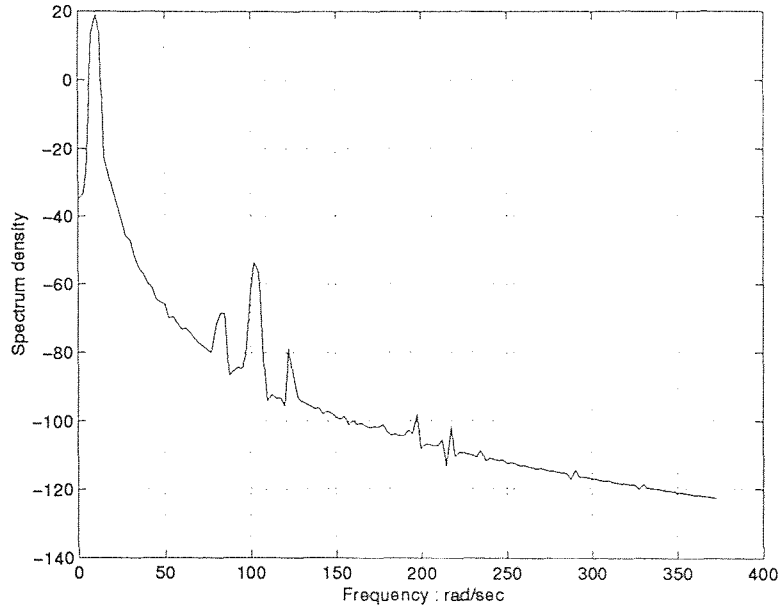

Figure 3.16 Spectral density of x_l

CHAPTER 4

COMPARISON OF PERFORMANCE OF DITHERED SYSTEM

4.1 Problem in Nonlinear System

A fundamental property of linear systems is scalability. That is, given a spectral $Y(\omega)$ due to input $X(\omega)$, then the spectral corresponding to $\alpha X(\omega)$ is given by $\alpha Y(\omega)$, where α is a positive scalar. This property, however, does not hold in a nonlinear system. For example, as discussed in Chapter 2, a nonlinear hysteresis model consists of two parts: (A) linear part : a second order linear system; (B) nonlinear part: multiloop hysteresis. Part (B) is memory dependent and maybe poorly known. Therefore in application, especially in precision control, this nonlinearity can adversely affect the system performance. With further analysis in frequency domain, it is found that PZT hysteresis causes harmonic distortion.

In this chapter, the properties of the dithered system will be compared to those of the nonlinear system as well as the linear portion of the original system. Two sets of tests will be carried out:

(A) Square wave test, where the steady-state output values of the above mentioned systems will be compared.

(B) Multiloop test, where it will be shown that the effects of the off-axis loops can be sufficiently reduced by means of a suitably chosen dither.

4.2 Properties of Linearized System

As shown in Chapter 3, when a suitable dither is injected into the nonlinear hysteresis model, the harmonic components are sufficiently attenuated, i.e. the system is "linearized". It is therefore of interest to determine the extend of linearization by

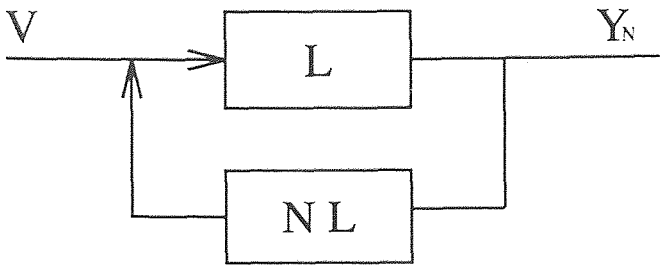

(I)

(II)

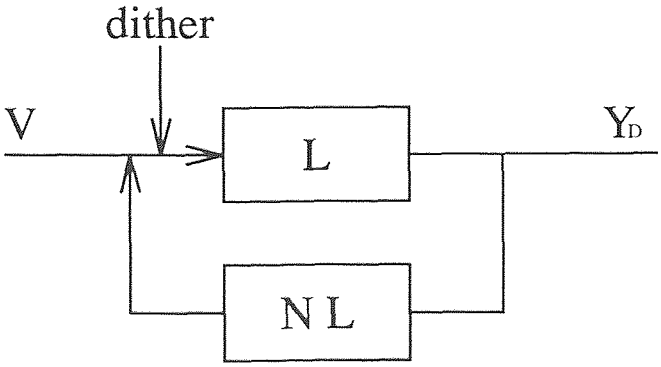

(III)

L : Linear part N L : Nonlinear part

Figure 4.1 Hysteresis model, ideal linear system and dithered system

comparing the dithered system to an ideal linear one. To facilitate the comparison, three systems are proposed as shown in Figure 4.1.

System (I) is the original nonlinear hysteresis model as shown on Figure 2.6 :

$$F_A = K_V V - \gamma \dot{x} - K_N x - K_1 F \tag{4.1}$$

System (II) is linear part of System (I), i.e. an ideal linear system:

$$F_A = K_V V - \gamma \dot{x} - K_N x \tag{4.2}$$

System (III) is a dithered system which is System (I) plus a dither.

$$F_A = K_V V - \gamma \dot{x} - K_N x - K_1 F + \delta \tag{4.3}$$

Where $F_A = M \ddot{x}$ and Y_N, Y_L and Y_D are respectively the outputs of Systems (I), (II) and (III) . V is input drive voltage. δ represents dither.

4.2.1 Square Wave Test

The purpose of the test is to determine the steady-state performance of the dithered system by comparing the tracking error between System (I), (II) and (III).

The input signal is a low frequency square wave with 25 second period and a 40 V amplitude as shown in Figure 4.2. The dither is $65sin103t$. Its amplitude is chosen by the adaptive mechanism which is now disable, i.e. the dither is injected on an open-loop basis. The outputs of the three models are plotted in Figure 4.3, where dashed line is the output of system (I), pointed line is that of system (II) and solid line is that of system (III). Defined now $e_1 = Y_N - Y_L$, $e_2 = Y_D - Y_L$ as the output deviation of the nonlinear and dithered nonlinear systems from the ideal linear part. The quantities are plotted in Figure 4.4 and Figure 4.5. It is observed that the nonlinear hysteresis force F causes a steady state error about ± 2.023 micrometer (17.6%) between Y_N and Y_L. For the dithered system, the steady state error between

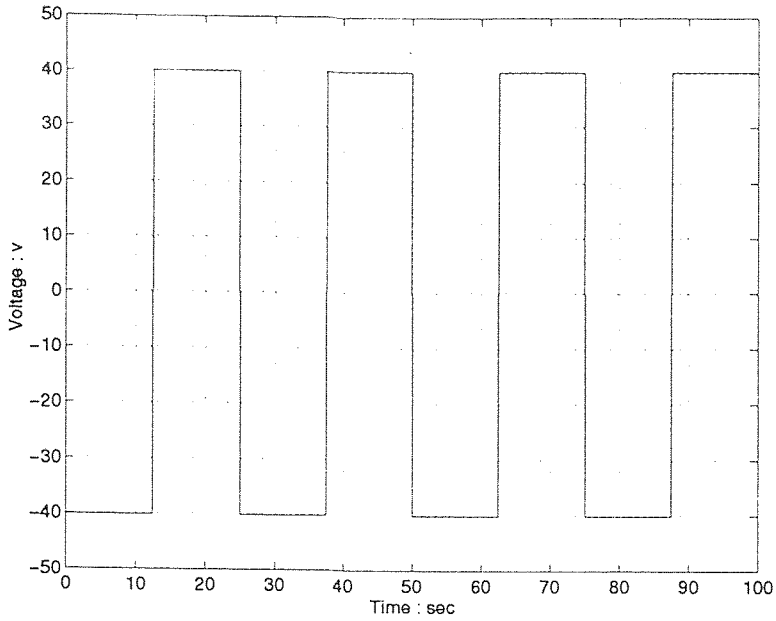

Figure 4.2 Square wave input

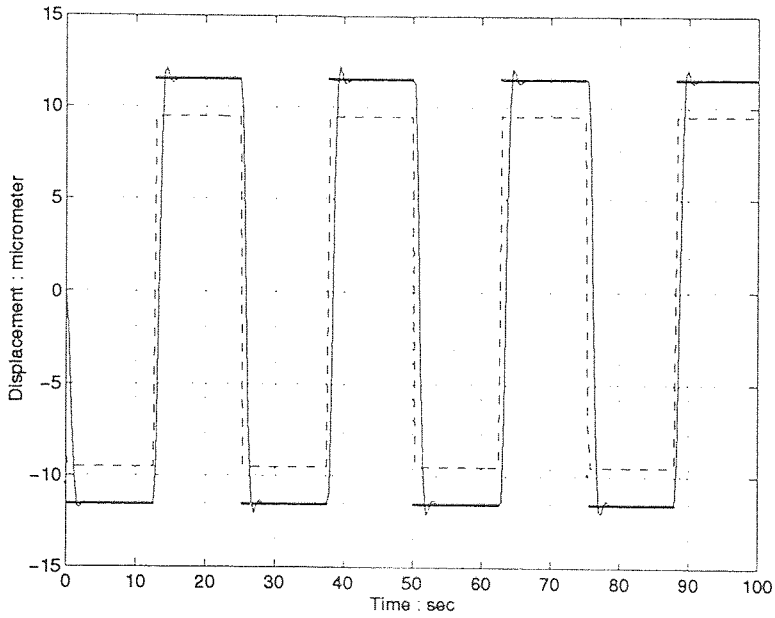

Figure 4.3 Output of system (I), (II) and (III) with same square wave input

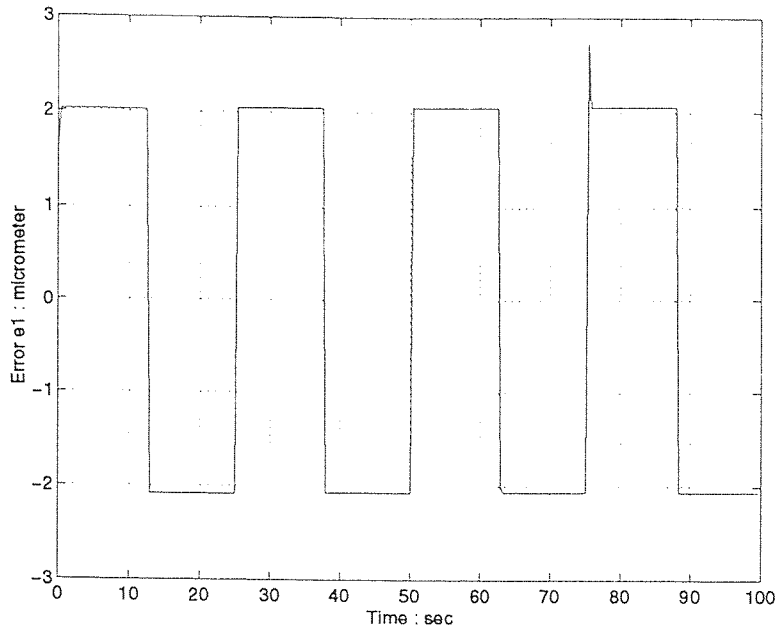

Figure 4.4 Error function of e_1

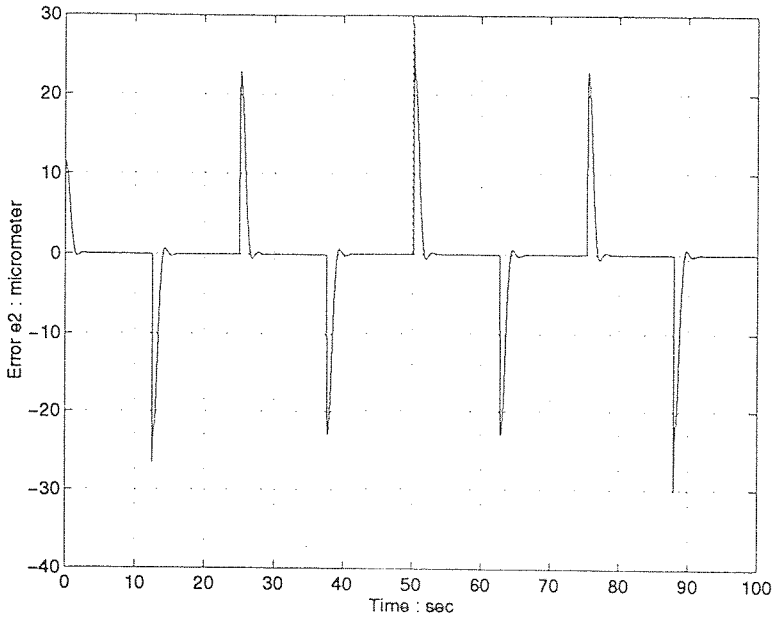

Figure 4.5 Error function of e_2

Y_D and Y_L is bounded by ± 0.019 micrometer (0.165%). in other words, the steady state error is reduced by more than 100 times by the dither, verifying the dither "linearized" hysteresis model quite well. The dithered system (III) is approximately "linear", it has almost the same characteristic as that of linear system (II). It should be noted that the "spikes" in e_2 (Figure 4.5) are due to the transient of the low pass filter. The low pass filter used here is a third order butterworth low pass filter with the cut-off frequency of 0.6 Hz.

4.2.2 Multiloop Test

In this section, it is desired to examine the effects of dither on the off-axis minor hysteresis loops. The configuration of the three systems: nonlinear, linear and dither-linearized remains as the same as in the previous section. The input voltage V however is now a composite sine wave as shown in Figure 4.6. For the nonlinear system this input signal effectively generate three hysteresis loops: one major loop and two minor off-axis loops as shown in Figure 4.7. The baseband response of the dither-linearized system is shown in Figure 4.8 which is almost the same as that of an ideal linear system as shown in Figure 4.9 (to compare under equal conditions, the same low pass filter is added to the ideal linear system. Since the low pass filter is linear, this will not affect the linearity comparison). It is observed that the undesired off-axis "memory" has been neutralized by the dither. The off-axis minor hysteresis loops now become ellipses that are symmetrical to the origin with the presence of dither.

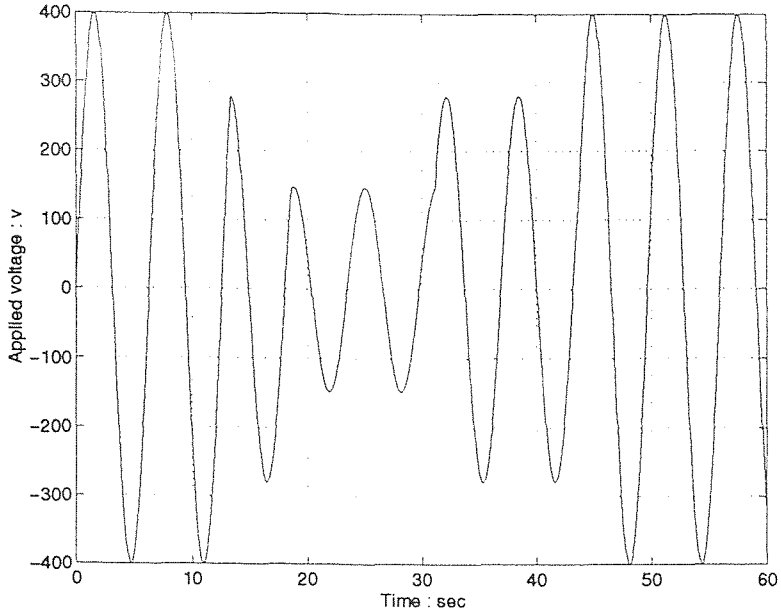

Figure 4.6 Input signal in multiloop test

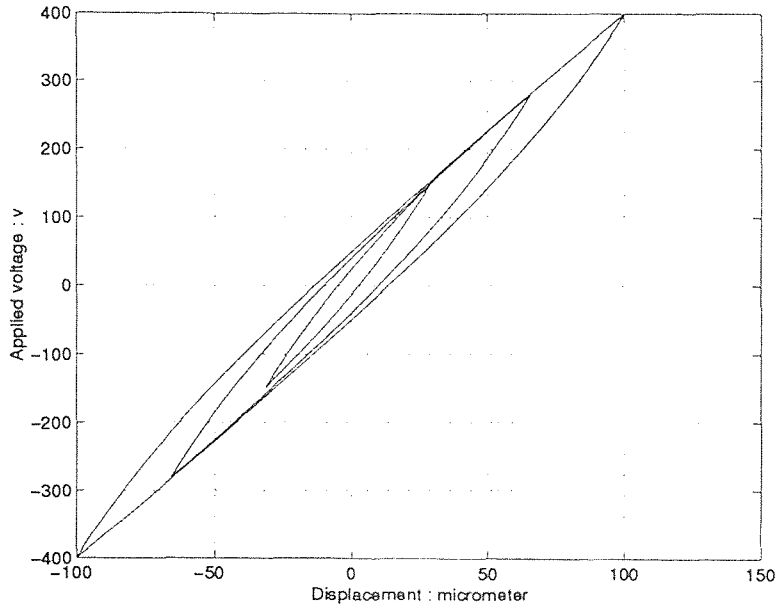

Figure 4.7 Multiloop situation

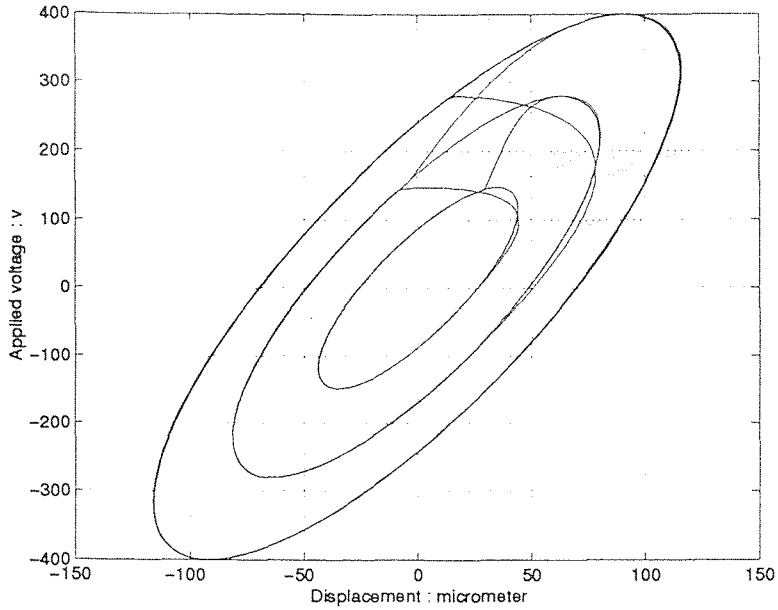

Figure 4.8 Lissajous's pattern of dithered system

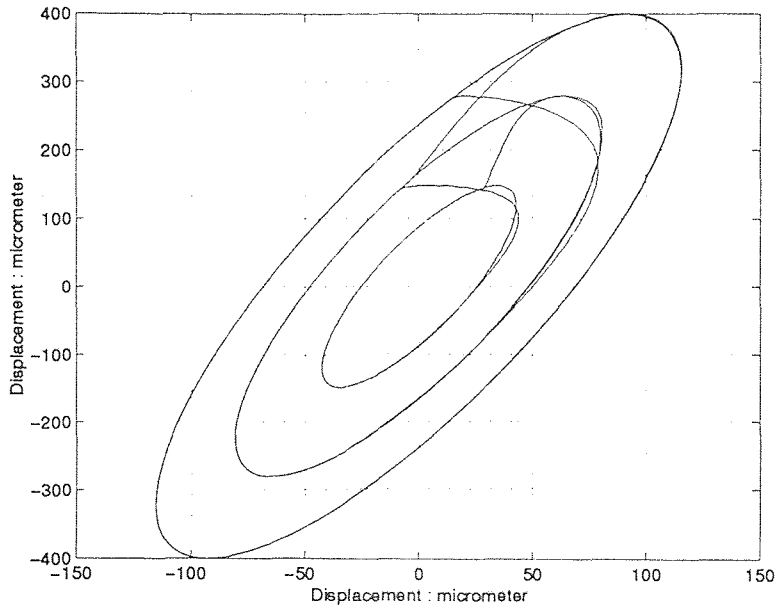

Figure 4.9 Lissajous's pattern of ideal linear system

CHAPTER 5

CONCLUSION

In this thesis, a nonlinear mathematical model of the PZT stack actuator is presented. It is based on Dahl's solid friction model [2] with the enhancement that it can accommodate different degrees of nonlinearity. The objective is to model and control nonlinear hysteresis loops, major and off-axis minor loops, formed between the applied voltage and PZT stack end displacement.

Extensive numerical simulations have been carried out to assess the characteristics of the PZT stack model. Once a suitable mathematical model has been obtained, a dither is injected to the model to attenuate the nonlinearity of the model. An adaptive system has been setup to find out a suitable amplitude of the dither to meet the requirement of a reference distortion ratio. Simulation results confirmed the effectiveness of dither in linearizing the PZT stack system. Furthermore, it is found that the adaptive mechanism is highly robust with satisfactory transient behavior.

The future work on control PZT stack can be suggested as follows:

1) Although a dither effectively linearized the hysteresis, it should be turned off when the PZT actuator displacement reaches the required end position. An optimal switching characteristic of the dither (e.g. at the zero crossing) should be studied.

2) Feedback control of the PZT stack position under adaptive dither should be carried out.

3) A more general and accurate mathematical model of hysteresis behavior remains a research topic.

APPENDIX A

Code of MatLab Functions Used in Simulation

A.1 Function INITIAL1.M

```
%this function should be run before simulation, it setup all the
%initial condition

global FEX
global true
global fl
global Fc
global FFc
global kk
global mm
global nn
global DFDX
global x_dot

%following 6 global varibles are use in function SPEC_COM.M

global nnn
global yy
global MM
global lll
global aa
global flag1

%following variable need an initial value before simulation

true=0;
fl=0;
nn=0;
kk=1;;
x_dot(1)=0.1;

MM=0.0014;
nnn=0;
aa(1)=0;
flag1=0;
```

```
point=2048
fd=30/2048
```

The meaning of those global variables in INITIAL1.M is following

nn : an index for each step of simulation;

FEX : hysteresis force at the Kth turnaround point;

True : an index shows simulation is in transient($true = 0$) or transient finished($true = 1$);

fl : an index for reset initial condition when transient finished;

Fc : hysteresis force at first loading point;

FFc : Hysteresis force at the point transient state finished;

kk : an index for Kth turnaround point;

mm : a variable record the variation of kk;

DFDX : $dF(x)/dx$;

x_dot : velocity;

aa : record for 2 points, let function check if the second point is a sample point;

nnn : an index for each sample point in function SPEC_COM.M

yy : a vector to record 512 points for spectrum density analysis;

MM : the output of the function SPEC_COM.M, namely the ratio of spectrum density

lll : the largest spectrum within 20 nearby points;

flag1 : an indicator to tell the function that 512 points are gottten and FFT is calculated.

A.2 Function INITIAL2.M

```
%initial purpose for multi-loop input, this file will generate a
%input signalused in simulate minor loop inside minor loop
%and the meaning of following variables are same as
%those in INITIAL1.M

global FEX
global true
global fl
global Fc
global FFc
global kk
global mm
global nn
global DFDX
global x_dot

T=linspace(0,45,1500);

t1=T(1:451);

t2=T(452:610);
t3=T(611:715);
t4=T(716:830);
t5=T(831:1500);

u1=sin(t1);
u2=-.7*sin(3*t2+1.7)+.125;
u3=.4*sin(4*t3-1.0)+.09;
u4=.7*sin(3*t4+1.7)+.125;
u5=sin(t5-5.25);

U=400*[u1 u2 u3 u4 u5]';
T=[t1 t2 t3 t4 t5]';

%above set up [T,U] workspace

true=0;
fl=0;
nn=0;


kk=1;
```

```
x_dot(1)=0.1;
point=2048;
fd=45/point;

plot(U),grid
```

A.3 Function MULTI.M

```
function  f=multi(uu)

%nn is a index for each step simulink call this function

nn=nn+1;

%if nn=1, it means simulation first tme call this function, so
%initial condition should be set, F is the hysteresis force.
%Fc is hysteresis force at first loading time. x_dot is the
%velocity.

if nn==1
F=uu(1);
Fc=5;
FEX(1)=-Fc*sgn(x_dot);
else
F=uu(1);
end

x_dot(2)=uu(2);

%if fl=1 means transient state finished and reset
%initial condition

if fl==1
Fc=FFc;
FEX(1)=-Fc*sgn(x_dot(2));
kk=1;
fl=0;
true=1;
end
```

```
%if true=0 means simulation is still in transient state,
%in the other hand true=1 means transient finished

if true==0

% check for turnaround point

if x_dot(2)*x_dot(1)<=0

%kk is the index for Kth turnaround point, and FEX(kk) is set
%when Kth turnaround point occur. mm is an index which
%indicate the times kk changes,we suppose after kk change
%4 times transient finished, and FFc is the hysteresis force at
%4th turnaround point, it will be the new Fc.

kk=kk+1;
FEX(kk)=F;
mm=[mm kk];
                                                KK=max(size(mm));
if KK==4
 fl=1;
 FFc=-F;
end
else

%kk > 2 means hysteresis loop possible

if kk>2
%next chech if minor loop closed or not, if closed kk=kk-2,
%revert to kk-2 curve

if abs(F-FEX(kk)) >= abs(FEX(kk)-FEX(kk-1))
kk=kk-2;
end

%check for first loading exceedance if exceed reset initial
%condition and the curve  will be the new k=1 curve

if kk<=2
if abs(F) > abs(FEX(2))
kk=1;
FEX(1)=-Fc*sgn(x_dot(2));
end
end
```

```
end
end
else

%following is for true=1,all others is same as above

if x_dot(2)*x_dot(1)<=0
kk=kk+1;
FEX(kk)=F;
else
if kk>2
if abs(F-FEX(kk)) >= abs(FEX(kk)-FEX(kk-1))
kk=kk-2;
end
if kk<=2
if abs(F) > abs(FEX(2))
kk=1;
FEX(1)=-Fc*sgn(x_dot(2));
end
end
end

end
end
%Prandtl law 1 and 3A is satisfied by the next equatio
DFDX=2-(F-FEX(kk))/Fc*sgn(x_dot(2));

%update x_dot
              x_dot(1)=x_dot(2);
%stiffness coefficient set to 5
f=5*DFDX;
```

A.4 Function AFFT.M

```
% for fft analysis a signal spectrum desity in db;
function afft(a,b,point);
x=hanning(point);
xx=a.*x;
Xdot=fft(xx);
mmag=20*log10(abs(Xdot(1:point/2)));
fs=1/b;
```

```
f=2*pi*fs/point*(0:(point/2-1));
plot(f,mmag),grid
xlabel('frequency : rad/sec')
ylabel('Spectrum density')
```

A.5 Function SPEC_COM.M

```
%this function compare the spectrum density in 2f , 3f, 4f ... 8f
%to that in f,which f is the frequency of the input signal, we
%pick the average of  3 most large spectrum in 2f, 3f ...8f,
%devided by that in f.

function z=spec_com(x);
%since we use a zero order hold before this function,
%so only when x changes its  this means we get next
%sample point
aa(2)=x;
if aa(2)==aa(1)
aa(2)=aa(2);
else
%nnn is an index for number of sample point, we will calculate
%spectrum density ratio every 512 points
nnn=nnn+1;
yy(nnn)=x;
aa(1)=aa(2);
end
if nnn==512
Y=fft(yy);
mag=abs(Y);
flag1=1;
nnn=0;
end
l=0;
%flag1=1 means we got 512 point and FFT result
if flag1==1
ll(1)=max(mag(19:23));
              ll(2)=max(mag(59:63));
              ll(3)=max(mag(99:103));
              ll(4)=max(mag(139:143));
s_max=sum(ll(2:4))/ll(1)/3;
z=s_max;
MM=z;
```

```
flag1=0;
else
z=MM;
end
%We here check 5 point around f,3f,5f,7f to make sure
%get the highest spectrum..
```

REFERENCES

1. P. R. Dahl, "Solid Friction Damping of Mechanical Vibrations," *AIAA*, vol. 14, Dec. 1976.

2. P. R. Dahl, "Math Model of Hysteresis in Piezo-electric Actuators for Precision Pointing Systems," El Segundo, California, Feb. 1985.

3. E. Grawley, "Use of Piezoelectric Actuators as Elements of Intelligent Structures," *AIAA*, vol. 25, pp. 1373–1385, 1987.

4. P. Halevi, "Bimorph Piezoelectric Flexible Mirror: Graphical Solution and Comparison with Experiment," *Opt. Soc. of Am*, vol. 73, pp. 110–113, 1983.

5. N. A. Osbourne and D. L. Rittenhouse, "The Modeling of Friction and Its Effects on Fine Pointing Control," *AIAA*, 1974.

6. H. S. Tzou, "Active Vibration Control of Flexible Structure via Converse Piezoelectricity," *Developments in Mechanics*, vol. 14-c, pp. 1201–1206, 1987.

7. D. Y. Abramovitch, F. Wang and G. F. Franklin, "Disk Drive Pivot Nonlinearity Modeling Part I: Frequency Domain," *Proceedings of the American Control Conference*, Baltimore, Maryland, 1994.

8. F. Wang, T. Hurst, D. Y. Abramovitch and G. F. Franklin, "Disk Drive Pivot Nonlinearity Modeling Part II: Time Domain," *Proceedings of the American Control conference*, Baltimore, Maryland 1994.

9. I. Alberto, *Nonlinear Control Systems: an Introduction* Berlin; New York: Spriger-verlag, 1989.

10. M. D. Bryant and R. F. Keltie, "A Characterization of the Linear and Nonlinear Dynamic Performance of a Practical Piezoelectric Actuator, Part 1 : Measurement," *Sensor & Actuators*, Vul No.9, 1986.

11. M. D. Bryant, "A Characterization of the Linear and Nonlinear Dynamic Performance of a Pactical Piezoelectric Actuator, Part 2 : Theory," *Sensor & Actuators*, Vul No.9, 1986.

12. R. C. Buchanan, "Ceramic Materials for Electronics," Tech. Rep., Marcel Dekker, 1980.

13. S. B. Choi, C. C. Cheong and S. H. Kim "Vibration Control of a Composite Beam Using a Distributed Piezofilm Actuator and Sensor," *Proceedings of the American Control Conference*, Baltimore, Maryland, 1994.

14. M. Fliess and M. Hazewinkel, *Algebra and Geometric Methods in Nonlinear Control Theory*, Boston: D. Reidel, 1986.

15. J. C. Hsu and A. U. Meyer, *Modern Control Priciples and Applications*, New York: Mcgraw Hill, 1968

16. I. J. Zeinoun and F. Khovromi,"An Adaptive Fuzzy Based Controller and Its Application to Smart Structures." *Proceedings of the 1994 American Control Conference*, Baltimore, MD, June 29 - July 1,1994.

17. R. R. Mohler, *Nonlinear Systems*, Englewood Cliffs, New Jersey: Prentice Hall, 1991.

18. "IEEE Standard on Piezoelectricity," The Institute of Electrical and Electronic Engineer Inc., 1978.

19. B. Jaffe "A Primer of Ferroelectricity and Piezoelectric Ceramics," Tech Rep., Bedford, Ohio, 1980